Thesis

Melphalan as a Potential Drug for the Treatment of Human Uveal Melanoma Evaluated in Chick Chorioallantoic Membrane

submitted by

Linda Wick, B.Sc.

in partial fulfillment of the requirements for the degree of

Doktorin der gesamten Heilkunde

(Dr^{in}. med. univ.)

at the

Medical University of Graz

executed at the

Division of Immunology

Department of Ophthalmology

under the supervision of

Nassim Ghaffari Tabrizi-Wizsy, Univ.-Ass. Priv.-Doz. Mag. Dr. rer. nat.

Christoph Schwab, Priv.-Doz. Dr. med. univ. Dr. scient. med.

Graz, 15.04.2024

Declaration of Academic Integrity

I hereby confirm that the present diploma thesis is the result of my own independent scholarly work. I also confirm that in all cases, where material from the work of others (in books, articles, essays, dissertations, and on the internet) is acknowledged, quotations and paraphrases are clearly indicated. No material other than that cited in the reference list has been used. I have read and understood the Medical University's regulations and procedures concerning plagiarism.

Graz, 15.04.2024 *Linda Wick m.p.*

Acknowledgements

First of all I would like to thank Univ.-Ass. Priv.-Doz. Mag. Dr. rer. nat. Nassim Ghaffari Tabrizy-Wizsy, without her hard work for the establishment of the CAM laboratory at the Medical University of Graz this thesis would not have been possible. Thank you for your encouragement and support as I took my first steps into medical research.

I would also like to thank Priv.-Doz. Dr. med. univ. Dr. scient. med. Christoph Schwab, a clinical expert in the field of ophthalmic oncology, for his ideas, motivation and guidance.

I am also very grateful to Pia Sophie Hysa for her expertise in cell culture. It was her irrepressible motivation that made this project possible. Thank you for your emotional and professional support in the laboratory!

In addition, I am grateful to Waltraud Huber and the entire team at the Otto Loewi Research Center for Vascular Biology, Immunology and Inflammation who warmly welcomed me and supported me in the laboratory.

Finally, I would like to thank my partner and my family at home for their motivating support, whicht went far beyond this work.

Zusammenfassung

Einleitung. Die Mortalität von Patient:innen mit Uveal Melanomen ist seit Jahren unverändert. Die Strahlen- und chirurgischen Therapien sind Methoden der Wahl, eine medikamentöse Therapie kann nicht angeboten werden. Melphalan wird bereits erfolgreich zur intraarteriellen Chemotherapie und zur intravitrealen Injektion bei Retinoblastomen eingesetzt, daher wäre es als potentielles Therapeutikum für das Uveal Melanom denkbar. Zur Erprobung ist das Chorioallantoismembran (CAM)-Modell geeignet, da es eine adäquate Grundlage für das Wachstum von Tumorzellen und dem Testen von potentiellen Medikamenten bietet.

Methoden. Befruchtete White Lohman Eier werden drei Tage inkubiert, geöffnet und in eine sterile Schale überführt. Nach einer weiteren Inkubation von sechs Tagen, werden vier etablierte UM Zelllinien (92.1, Mel270, OMM-2.3, OMM-1) auf die CAM der Embryonen verpflanzt. Einen Tag später wird je 10µl Melphalan mit einer Konzentration von 10µg/mL auf die Zellen gegeben. Nach drei Tagen werden die Tumore fotodokumentiert, ausgeschnitten und histologisch aufgearbeitet. Neben der morphologischen Betrachtung wird die Mitose der Tumorzellen mit Hilfe des Mitosemarker Ki-67 immunhistologisch analysiert. Zuvor wurde in einem vorangegangenen Experiment die passende Matrix für die Uveal Melanom Zelllinien bestimmt.

Ergebnisse. Alle vier Uveal Melanom Zelllinien wachsen auf der CAM und bilden unter dem Einfluss von Matrigel teils bräunlich pigmentierte Tumore, die von CAM-Blutgefäßen durchwachsen werden. Für die Zelllinie 92.1 lassen sich makroskopisch Unterschiede zwischen den behandelten und unbehandelten Zellen erkennen. Die histologischen Färbungen zeigen, dass die Tumorzellen unter dem Einfluss von Melphalan weniger mitotisch aktiv sind und viele Zellen bereits absterben. Das CAM Gewebe dagegen ist unverändert.

Diskussion. Das CAM-Modell stellt eine valide Option zur Untersuchung der Fragestellung dar und die aktuellen Ergebnisse bestärken einen ersten aussichtsvollen Ansatz in der Therapie des Uveal Melanoms. In Zukunft werden weitere Untersuchungen benötigt, um die Wirkung von Melphalan auf Uveal Melanom Tumore besser verstehen zu können.

Abstract

Introduction. The mortality rate of patients with uveal melanoma has remained unchanged for years. Radiotherapy and surgical treatment are the methods of choice; drug therapy cannot be offered. Melphalan is already being used successfully for intra-arterial chemotherapy and intravitreal injection for retinoblastoma, so it could be a potential therapeutic agent for uveal melanoma. The chorioallantoic membrane (CAM) model is suitable for testing, as it provides an adequate basis for the growth of tumour cells and the testing of potential drugs.

Methods. Fertilised White Lohman eggs are incubated for three days, opened and transferred to a sterile dish. After a further incubation period of six days, four established UM cell lines (92.1, Mel270, OMM-2.3, OMM-1) are transplanted onto the CAM of the embryos. One day later, 10µl of Melphalan at a concentration of 10µg/mL is added to onplant. After three days, the xenografts are photodocumented, excised and histologically processed. In addition to morphological observation, the mitosis of the tumour cells is analysed immunohistologically using the mitotic marker Ki-67. Prior to this, the appropriate matrix for the uveal melanoma cell lines was determined in a previous experiment.

Results. All four uveal melanoma cell lines grow on the CAM and, under the influence of Matrigel, form partly brownish pigmented tumours that are permeated by CAM blood vessels. For cell line 92.1, macroscopic differences between the treated and untreated cells can be recognised. The histological staining shows that the tumour cells are less mitotically active under the influence of Melphalan and that many cells are already dying. The CAM tissue, on the other hand, is unchanged.

Discussion. The CAM model represents a valid option for investigating the issue and the current results confirm a promising initial approach in the treatment of uveal melanoma. Further studies are needed in the future to better understand the effect of Melphalan on uveal melanoma tumours.

Table of Content

List of Abbreviations

BAP1	BRCA1 associated protein 1
BRAF	b- rapidly accelerated fibrosarcoma
CAM	chorioallantoic membrane
CK	cytokeratin
CYSLTR2	cysteinyl leukotriene receptor 2
DNA	deoxyribonucleic acid
EIF1AX	eukaryotic translation initiation factor 1A X-linked
EtOH	ethanol
FBS	fetal bovine serum
GNAQ	g protein subunit alpha q
GNA11	g protein subunit alpha 11
HE	hematoxylin eosin
mRNA	messenger ribonucleic acid
NF1	neurofibromin 1
NRAS	neuroblastoma RAS
p	passage
PBS	phosphate buffer saline
PLCB4	phospholipase C beta 4
P/S	penicillin/streptomycin
RPMI	Roswell Park Memorial Institute
RT	room temperature
SF3B1	splicing factor 3b subunit 1

List of Figures

List of Tables

1. Introduction

1.1. Respective Uveal Architecture

1.1.1. Anatomy

Looking at the eye in sagittal section, three layers are distinguished: the outer, middle and inner layer. The vascularised middle ocular membrane is made up of the choroid, ciliary body and iris stroma and is also known as the uvea. It supplies the outer parts of the retina with oxygen and, among other things, forms the aqueous humour.

In terms of developmental history, the iris comprises two parts, the iris epithelium and the iris stroma, whereby the former forms a pigmented part of the inner skin of the eye, the retina. The iris stroma consists mainly of connective tissue and contains melanocytes, which produce different amounts of melanin depending on the colour of the eye. If a person has a lot of melanin in the iris stroma, the eyes will appear brownish in colour macroscopically. Blue, green and grey eyes appear in people with less melanin in the iris stroma. In addition to the connective tissue and the melanocytes, the iris stroma is traversed by vessels that primarily supply the tissue with oxygen.

The ciliary body stretches like a ring inside the eye and is mainly formed by the ciliary muscle, which is covered by the ciliary epithelium. The main functions of the ciliary body are to participate in the accommodation of the lens and the formation of the aqueous humour. The ciliary epithelium is two-layered, its outer side, which borders on connective tissue rich in blood vessels, is pigmented, the inner side is not.

The choroid itself is part of the posterior segment of the eye and can be divided from the inside out into the choriocapillaris, vascular stratum and suprachoroidea. All layers consist mainly of blood vessels surrounded by loose connective tissue and numerous melanocytes (Welsch et al., 2022:603-613).

1.1.2. Function of Melanocytes

Already during embryogenesis, melanocytic precursor cells, the so-called melanoblasts, migrate from the neural crest into the skin (Sommer, 2011:411-413). Here they then begin to produce melanin. Tyrosine is produced from phenylalanine, which is required for the production of melanosomes. Melanosomes are specialised organelles of the melanocytes in which the pigment melanin is stored (Schallreuter et al., 2008:396-398). The melanosomes are released in the epidermal melanocyte unit to the surrounding keratinocytes to protect

them primarily from harmful UV radiation. However, melanocytes are not only found in organs exposed to UV light, such as the skin, but also in the eye, the inner ear and the intestinal mucosa. Yamaguchi & Hearing (2014:2) provide evidence that melanocytes in animal models in these organs present themselves differently to various stimuli than epidermal melanocytes. However, the function of those in these tissues is not fully understood. In the choroid of the eye, for example, there is a positive correlation between the number of melanocytes and the diameter of the choroid; patients with vitiligo, an autoimmune disease that attacks the melanocytes, show a smaller choroidal diameter (Demirkan et al., 2018:3). This correlation could possibly be explained by the fact that melanocytes induce angiogenesis and thus influence the thickness of the choroid, which is rich in blood vessels. The absence of melanocytes in the eye and inner ear are also associated with microphthalmia and sensorineural hearing loss, respectively, which also sheds light on their important role in development and angiogenesis (Schatz et al., 2019:1-3).

1.2. Uveal Melanoma

Although it represents the most common intraocular tumour, uveal melanoma is a rare malignancy of the uveal tract with an incidence of 6.41 new cases per one million inhabitants (Alfaar et al., 2022: 1730). Across Europe, there is a north-south gradient, with an incidence of >8 new cases per one million Norwegians and <2 new cases per one million Spaniards (Virgili et al., 2007:2309). Three localizations are distinguished depending on the section of the uveal tract, each accounting for a different frequency proportion of the diagnosis. The most commonly affected is the choroid with 80% followed by the corpus ciliare with 12% and the iris with 8% (Salmon, 2019:847, 843, 841).

1.2.1. Pathogenesis and Genetical Characteristics

Uveal melanoma develops from melanocytes of the uvea and represents the second most common localization of melanoma (Chang et al. 1998:1666). Compared to cutaneous melanoma, which is mainly characterized by mutations in BRAF, NRAS, KIT and NF1, uveal melanoma has different genetic characteristics as well as a lower mutational burden (Davis et al. 2018: 3491).

In studies of uveal melanoma tumors, a mutation of the G proteins has been observed in more than 80% of cases. These proteins are involved in the communication of a cell with its environment and play a crucial role in this signal transduction pathway. For uveal melanoma

in particular, two mutations in the alpha subunit, GNAQ and GNA11, have been identified. These mutations are referred to as driver mutations for uveal melanoma and initiate pathogenesis through cell proliferation, but have no influence on mortality or the risk of metastasis (Van Raamsdonk et al., 2009:599-601, Van Raamsdonk et al., 2010:2192-2195). Furthermore, mutations in CYSLTR2 or PLCB4 were also discovered, which play a similar role to GNAQ/GNA11 and are involved in the same signal transduction pathway, thus emphasizing its relevance for the development of uveal melanoma (Moore et al., 2016:1, Johannson et al., 2016:4625).

In addition to the mutations mentioned above, which mainly affect the development of uveal melanoma at the beginning, there are further mutations that manifest themselves later in the course of the disease yet have a decisive influence on the prognosis. Depending on the mutation, a distinction is made between high-risk mutations, intermediate and low-risk mutations, which entail a different risk of metastasis.

The pathway of high-risk mutations is characterized by the development of monosomy 3 (Bechrakis et al., 2021:762, Tschentscher et al., 2003:2578-2584). This is important because the third chromosome codes for the BAP1 protein, which acts as a tumor suppressor protein (Jensen et al., 1998:1098). The tasks of the BAP1 protein include interacting with other proteins and enzymes to repair damaged DNA or, if necessary, initiate apoptosis, meaning controlled cell death (Han et al., 2021:751, Bultynck and Campanella, 2017:76). If an additional inactivating mutation of the remaining BAP1 gene is added to monosomy 3, a defective cell cycle as well as uncontrolled cell proliferation occur, which catalyze the malignant degeneration of the cells. These tumors often show an epithelioid cell appearance, which is also associated with an aggressive phenotype (Koopmans et al., 2014:1326-1327). A comparison of the literature shows that around 33% to 45% of all patients with uveal melanoma have BAP1 inactivation; if patients who have already developed metastases are considered, this mutation is present in >70% of cases (Decatur et al., 2016:3, Lamas et al., 2021:4). These results suggest that BAP1 inactivation is more frequently associated with metastasis. Koopmans et al. (2014:1328) investigated this connection and were able to report an eightfold increase in the risk of metastasis, which has a significant impact on prognosis. Based on a period of five years, there is a significantly increased mortality of 55% in patients whose tumors do not express the tumor suppressor protein compared to 0% in patients whose tumors express BAP1 (Van de Nes et al., 2016:803). This increased mortality is mainly due to the formation of distant metastases. In the case of uveal melanoma, these mainly spread

to the liver, less frequently to the lungs and bones, and usually lead to the death of the patient within one year (Lamas et al., 2021:4, Diener-West et al., 2005:1640).

Regarding genetics, there is another factor associated with the high-risk pathway. An analysis by Van den Bosch et al. (2012:2669) shows additional copies of the longer chromosome arm of the 8th chromosome (gain of 8q), which lead to a more aggressive course of the disease and metastasis as the number of copies increases. The exact mechanism of this process is not yet fully understood, but it is suspected that the proto-oncogenes localized on 8q are involved (Amaro et al.,2017:118).

A disomy of the third chromosome is always a prerequisite for both the low and the intermediate risk pathway. The most important low-risk mutation would be the EIF1AX mutation. The gene in question codes for a translation initiation factor and is required for the attachment of ribosomes to RNA (National Library of Medicine, 2023). The mutation occurs in approximately half of all uveal melanomas with inconspicuous chromosome 3 status and is associated with a low metastatic potential (Martin et al., 2013:933). A study by Ewens et al. (2014:5164) indicates that patients with an EIF1AX mutation have an 87% lower risk of metastasis than patients whose tumors do not harbor this mutation, suggesting a protective effect on the course of the disease. The actual mechanism by which this mutation reduces the risk of metastasis is not fully understood, however, this connection could play an important role in the future with regard to treatment options and preventing the spreading of disease.

A mutation in the gene coding for the protein SF3B1 is associated with the intermediate pathway. This protein is involved in the process of splicing, in which the non-coding regions of the RNA strand, known as introns, are removed to form the mature mRNA (National Library of Medicine, 2024). A study by Martin et al. (2013:933) showed that around one third of all uveal melanomas with disomy three harbor this mutation, and that this mutation is also increasingly observed in younger patients (Decatur et al., 2016:3). Characteristically, these tumors do not metastasize within the first two years, but only later in the course of the disease and less frequently, which significantly improves the prognosis (Yavuzyigitoglu et al., 2016:1118-1128).

Interestingly, the respective "second hit" mutations occur mutually exclusive, indicating that most patients harbor either the BAP1 mutation, EIF1AX mutation or SF3B1 mutation, but rarely combinations of those (Decatur et al., 2016:3, Lamas et al.,2021:4). Overall, the

genetic profile of uveal melanoma is an important predictor for the prognosis of the respective patient, especially since only <5% of all patients have metastases at diagnosis (Chattopadhyay et al., 2016:2302). Depending on the genetics of the tumor, close follow-up is strongly recommended for patients in order to detect metastases as early as possible.

1.2.2. Host Susceptibility and Associated Conditions

Despite the potentially different localizations of uveal melanoma and their frequency, these subtypes have similarities in terms of their host susceptibility and their associated conditions. According to a meta-analysis by Weis et al. (2006:57), uveal melanoma occurs more frequently in people with light skin color and light iris color as well as in people with an inability to tan. A correlation with hair color could not be statistically proven. The authors suggest two possible interpretations of their results. On the one hand, the eye could be less protected from UV radiation due to the different pigmentation, and on the other hand, a melanin-independent factor is suspected that leads to an increased incidence of uveal melanomas in this subpopulation.

As uveal melanoma can develop from an intraocular nevus, an association between the two is assumed (Salmon, 2019:840, 846). In contrast, the connection between uveal melanoma and cutaneous nevi or freckles was controversial, as the study situation seemed ambiguous. Weis et al. (2009) addressed this issue in a comprehensive meta-analysis and were able to describe a higher incidence of uveal melanoma in patients with multiple cutaneous nevi, atypical cutaneous nevi, cutaneous freckles and iris nevi. These results indicate the importance of UV light exposure. Several studies have shown a correlation between UV light exposure and the increased occurrence of cutaneous nevi, especially in young people during their first two decades of life (Bauer et al., 2005:125; Breitbart et al., 1997:376). Combining this tendency for the formation of new nevi with the findings that UV light can penetrate to the choroid, especially within the first decade of life, there might be a potentially critical period for the later development of uveal melanomas especially in the childhood years (Mallet et al., 2013:17). This hypothesis is supported by the fact that choroidal nevi are mainly newly diagnosed until late childhood and rarely in adults (Salmon, 2019:846).

As a special form of nevus, melanocytoma is associated with a 1-2% risk of malignant transformation and thus also represents a condition that is associated with an increased incidence of uveal melanoma. (Shields et al., 2019:1951-1953, Salmon, 2019:841). Furthermore, uveal melanoma occurs more frequently in patients with congential ocular and

oculodermal melanocytosis. This condition is associated with an increased number, size and pigmentation of melanocytes in the uvea and sclera, which presumably also leads to the increased incidence of uveal melanoma in these patients (Salmon, 2019:302).

BAP1 tumor predisposition syndrome is an autosomal dominant hereditary disease that leads to inactivation of the tumor suppressor gene BAP-1. This group of patients already has a genetically increased risk of developing uveal melanoma, various skin tumors or malignant mesothelioma (Abdel-Rahman et al., 2011:858). Interestingly, there is a significantly lower risk of developing metastases in this syndrome compared to patients with somatic BAP1 mutations (Ewens et al., 2018:9). There is no definitive explanation for these results, but Ewens et al. (2018:9) suspect that the somatic tumor mutations are more aggressive in behavior because they form late in the course of tumor development and should therefore be viewed differently from germline mutations in the tumor predisposition syndrome.

1.2.3. Treatment

In recent years, the approach to the treatment of uveal melanoma has increasingly shifted towards a globe-preserving strategy. The main goals of primary tumor therapy are local tumor control and preservation of visual acuity and the eye (Bechrakis et al., 2021:762-769). Various therapies and possible targets for uveal melanoma are currently being researched in order to improve the prognosis of patients.

1.2.3.1. Treatment Options

Both radiotherapy and surgical therapy are available for uveal melanoma, whereby combinations of both can be used. In addition to brachytherapy, in which beta or gamma radiation is used depending on the tumor thickness, proton therapy, gamma knife and LINAC irradiation are also used. Depending on the choice of treatment method, local tumor control can be achieved in 90%-98.3% of cases within a period of five years (Jampol et al., 2020:154). The disadvantage of radiation procedures is that the majority of patients develop radiation-induced retinopathy over time, which further impairs the visual acuity of the eye (Rauchegger et al., 2020:21-22).

From a surgical perspective, a distinction is made between two different methods, endoresection and enucleation. Endoresection is offered by specialized tumor centers such as the Charité in Berlin and aims to remove the entire tumor without damaging other structures. In the case of advanced lesions, there is an indication for enucleation, in which the eye must be removed in its entirety and replaced with a prosthesis. The appropriate choice

of treatment depends on tumor thickness, tumor location, physical condition of the patient and concomitant diseases and should always be made together with the patient in order to achieve the best possible results (Bechrakis et al., 2021:762-769).

1.2.3.2. Potential Drug: Melphalan

Melphalan, or L-phenylalanine mustard, is a synthetic cytostatic drug that was recognised in the early days as having a particular affinity for malignant melanomas. One of the reasons for this is the increased consumption of phenylalanine and tyrosine specifically for melanomas, which leads to an increased accumulation of the active substance in those cells due to the structure of Melphalan (Bergel & Stock, 1953, cited in Samuels & Bitran, 1995:1786). Melphalan acts as an alkylan, which leads to the intracellular cross-linking of both DNA strands and thus impairs cell replication. In this context, Benathan et al. (1992:311-312) focussed on the effect of Melphalan on melanoma cells. They were able to show that pigmented melanoma cells react more sensitively to the active substance than amelanotic melanoma cells. The authors believe that this is due to a melanin-induced deviation in the intracellular redox balance, which contributes to these results.

Melphalan is already used in the treatment of ophthalmological tumours and metastases in addition to its numerous other applications. For example, if there is vitreous seeding in the context of a retinoblastoma, this can be treated locally with intravitreal injections of Melphalan. In their study, Munier et al. (2012:4) were able to achieve local tumour control in >90% of patients after four injections with Melphalan. These extremely positive results were also replicated in research by Shields et al. (2016:1190), in which tumour control was achieved in 100% of cases after 3 years. There is also the option of intra-arterial injection with Melphalan for retinoblastoma. The drug is primarily used for more advanced tumours, as the method of application ensures a higher local drug concentration compared to intravenous application (Shields et al., 2012: 203-207). For the treatment, a catheter is placed in the femoral artery, which is guided into the vascular system in the caudal direction to the ophthalmic artery. Melphalan is then applied locally. Overall, this procedure has proven to be effective, with topotecan and carboplatin being applied in addition to Melphalan in order to maximise the therapeutic effect (Gobin, 2011:733-737). Another procedure, known as isolated hepatic perfusion, utilises a similar principle in the battle against liver metastases in uveal melanoma. In this treatment, Melphalan is administered in high doses into the hepatic artery in order to minimise the risk of systemic side effects. Olofsson et al.

(2023:3044-3048) report a significantly better response and longer progression-free survival in patients who have received this treatment. Overall, Melphalan covers a broad spectrum of diseases from an ophthalmooncological perspective, which is why its use in the treatment of the primary tumour of uveal melanoma is conceivable.

1.3. CAM Model, Advantages and Significance for Cancer Research

The chorioallantoic membrane (CAM) is a vascularised and nutrient-rich membrane that develops during the embryogenesis of avian species and has been studied for several decades. Microscopically, the membrane is composed of two epithelia connected by vascularised mesenchyme (Ribatti, 2014:2). The CAM develops three days after fertilisation of the eggs and fulfils vital tasks for the embryo. It ensures gas exchange as well as the removal of waste products from the embryo and supplies it with energy and fluids (Ribatti, 2016:1-8). CAM is primarily researched in chickens, in this context the period from fertilisation to hatching is 21 days, whereby most experiments are completed after 13-16 days, as the embryo's immune system develops during this period (Romanoff, 1960 cited in Ribatti, 2014:2, Janković et al., 1975:500-507, Mesas et al., 2024:17).

This is one of the major advantages of the CAM model, particularly in the context of cancer research, as the embryo is immunodeficient within the first two weeks. This makes it possible to transplant human cells and xenografts onto the membrane, as these cannot be rejected due to immune response. Many types of cancer, including glioblastoma, medullary thyroid cancer, pancreatic carcinoma, renal cell carcinoma and melanoma, have already been investigated (Strojnik et al., 2010:4851-4860, Ghaffari-Tabrizi-Wizsy et al., 2009:462-467, Zhao et al., 2018:1440-1452, Fergelot et al., 2013:181-194, Rinner et al., 2017:2-5). Various uveal melanoma cell lines as well as patient derived tumour xenografts were also successfully transplanted and researched on the CAM (Sokolenko et al., 2022:5-9, Tsimpaki et al., 2023:7-15). In both experiments, the in ovo technique was used, which means that the CAM is accessed via a small window in the eggshell. To my knowledge, research in the sense of an ex ovo variant, i.e. without a shell, has not been carried out before.

CAM research has proved particularly useful in connection with the major hallmarks of cancer such as angiogenesis, proliferation, invasion and metastasis. In addition, the superficial localisation of tumours on the CAM makes it possible to test potential active substances and identify macroscopic differences. A systematic review by Mesas et al.

(2024:4-26) analysed 74 papers and showed that CAM is an established in vivo method for investigating the behaviour of different cancer cells with and without the influence of potential therapeutic agents and provides a valuable alternative to rodent experiments. Furthermore, the experiments are quickly reproducible due to their short duration and research questions can be answered comprehensively in a short time with several repetitions of the same experiment. In addition, apart from incubators for the eggs, no special equipment is required for research on the CAM, which makes this method particularly cost-effective and beginner-friendly.

1.4. Study Aims and Hypothesis

This study is divided into two consecutive sub-experiments.

The first aims to investigate under which matrix condition (Medium, Matrigel®, Geltrex™) the respective uveal melanoma cell lines (92.1, OMM-1, OMM-2.3, Mel270) grow and successfully form tumours that are big, vascularized and adhesive to the CAM using the ex ovo method. The literature suggests that Matrigel® is the most promising matrix (Sokolenko et al., 2022:5-9, Tsimpaki et al., 2023:7-15). The results are assessed descriptively macroscopically and microscopically with the aid of histological staining.

In the second part, the potential therapeutic agent Melphalan will be applied to the cells as part of a pilot trial in order to investigate its effect. A subsequent descriptive assessment of the macroscopic and microscopic changes will be carried out with the aid of histological staining.

Hypothesis:

Under the Influence of Matrigel®, uveal melanoma cell lines develop the largest tumours.

Uveal melanoma cell lines (92.1, OMM-1, Mel270, OMM-2.3) which are treated with Melphalan show more signs of cell death than uveal melanoma cell lines which are not treated.

2. Material and Methods

All materials and methods used are explained below. A total of two consecutive experiments were carried out, a schematic representation of the most important milestones of the two experiments can be seen in figure 1. Work on the chicken eggs was always carried out with gloves and FFP2 masks to reduce the risk of contamination.

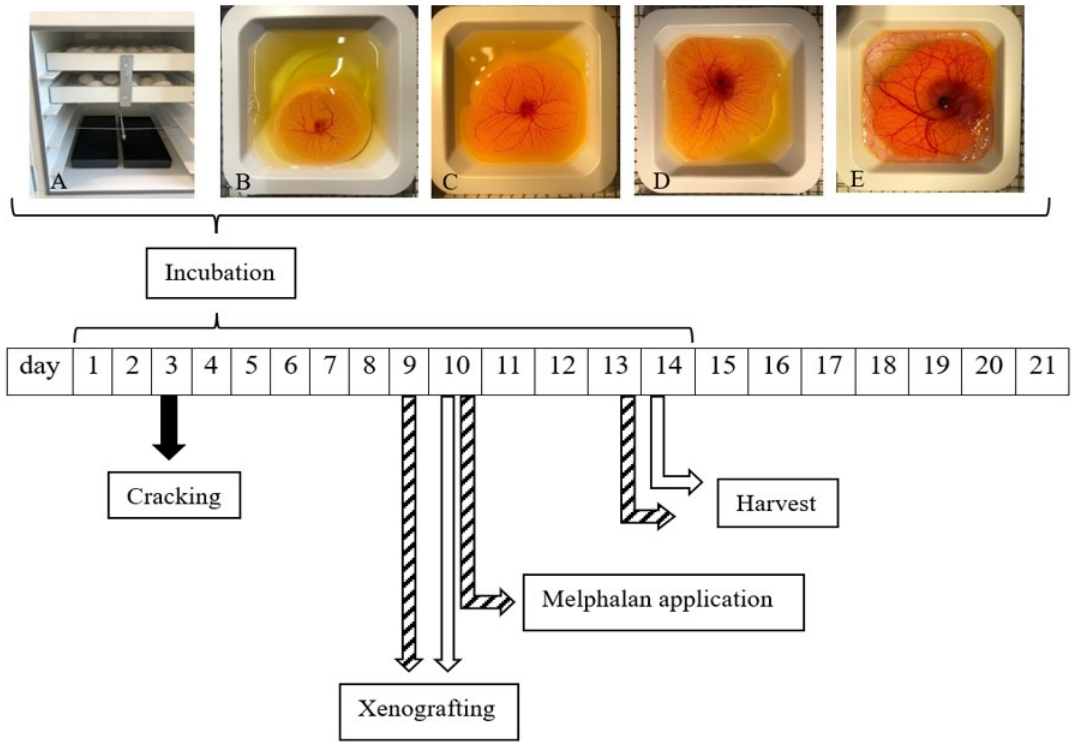

Figure 1. Chronological and schematic workflow of the ex-ovo CAM assay for the first and second experiment. The number line represents the days of the experiments. The eggs were incubated again after each step. (A) After cleaning, the eggs were put in the incubator on the day of arrival. On the third day, the eggs were freed from their shells, see black arrow. (B)- (D) Development of the CAM from day four to six, whereby the vascularisation, the size of the embryo as well as the size of the yolk sac increases continuously. (E) The chick embryo on day ten as it appears when ready for xenografting. The white arrows represent the most important steps of the first experiment, while the striped arrows represent those of the second experiment. In the second experiment, Melphalan was applied on day ten, one day post xenografting. After harvesting, the xenografts were fixed and histologically processed.

2.1. Uveal Melanoma Cell Lines

Respective cell lines were stored in the nitrogen tank until the time of the experiment. For cell culture work the sterile bench HERASAFE KS from Thermo Scientific was used. After thawing, the cells were cultured with the aim of gaining an understanding of the different cell lines in their growth cycle so that enough living cells would be available for our experiments. Aliquots of RPMI-1640 medium with L-glutamine mixed with 10% FBS as well as 1% P/S were used as culture medium as recommended by White et al. (2006:12) and

Amirouchene-Angelozzi et al. (2014:1510). Cells were incubated in cell culture incubator (Thermo scientific BBD 6220 CO_2 Incubator) at 37°C, 4.2%CO_2 and 85% relative Humidity. An overview of the most important aspects of the respective cell lines can be found in table 1. All cell lines were regularly checked macroscopically as well as microscopically for contamination. The photos of the cell lines were taken with the Olympus CKX53 microscope with built-in UC90 microscope camera using cellSens software. To count the cells and check their viability, cells were centrifuged (Heraeus Instruments Megafuge 2.0) at 1200 rpm for four minutes and counted using the Casy TTT (OMNI Life Science GmbH & Co. KG) cell counting and analysing system.

Table 1. *Overview of the most important aspects of respective cell lines. Cell line Mel270 and OMM-2.3 originated from the same human being.*

cell line	92.1	OMM-1	Mel270	OMM-2.3
organism	human	human	human	human
cell origin	choroid	skin metastasis	choroid	liver metastasis
age (years)	76	74	79	80
gender	female	male	male	male
culture	adherent	semi-adherent	adherent	adherent
splitting ratio and frequency	1:4.5 every two days	1:3 every two days	1:4.5 every two days	1:4.5 every three days
genetic aberrations	GNAQ, Gain 8q, EIF1AX	GNA11, triploid chromosome set	GNAQ, tetrasomy 6p	GNAQ

2.1.1. Cell Line 92.1

This cell line was originally derived in The Netherlands from the primary tumor of a 76-year-old female patient suffering from uveal melanoma. On admission, the patient was diagnosed with amaurosis which developed as a result of the extensive tumor growth. The tumor, which originated from the choroid, infiltrated the optic nerve and eye muscles as reported by De Waard-Sieblinga et al. (1995:155). After the patient's death 2.5 years later, several metastases were discovered, including in the heart, liver and adrenal gland (Jager et al. 2016:3).

Jager et al. (2016:4) looked at the genetic profile of cell line 92.1 and confirmed a GNAQ mutation and a gain of 8q, as well as a disomy of chromosome 3. A BAP1 mutation could not be confirmed. Similar results were obtained by Amirouchene-Angelozzi et al. (2014:1512), who were also able to describe a mutation in the EIF1AX gene.

For the experiment we thawed 5 x 10^6 Cells with a passage of 4. In routine cell culture, the cells proved to be adherent as they were able to attach very well to the culture vessel surface as shown in figure 2A. Amirouchene-Angelozzi et al. (2014:1512) assumed a doubling time of 38h which is consistent with the perception of the growth kinetics of our cells. On average, cells were split 1:4.5 every 2 days with an observed confluence of 80-90%. In the light microscope, the cells appear pleomorphic with predominantly multipolar cell bodies, which show several dendrite-like extensions. As shown in figure 2B, at 400x magnification, the melanin pigmentation is visible as granules as well as the prominent nucleoli.

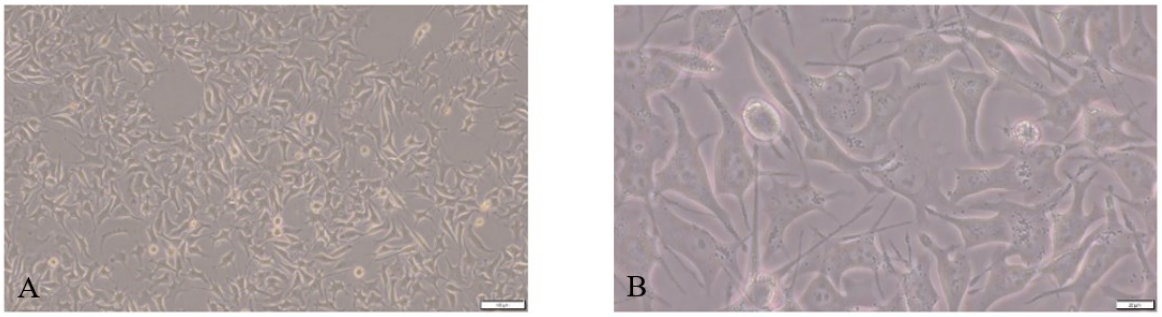

Figure 2. Cell line 92.1, passage 5, (A) 100x magnification, (B) 400x magnification, scale bar: 20µm.

For the first experiment we were able to obtain 5,7x 10^6 Cells, p7 and a viability of 76,5% and for the second experiment we were able to obtain 14 x 10^6 cells, p11 and a viability of 79,4%. Table 2 shows the cell numbers, passage and viability at respective measuring points.

Table 2. *Cell count, passage and viability of the cell line 92.1 in relation to the different measuring points. nd =not determined*

92.1	Measuring points	Cell count	Passage	Viability in %
	Thawing	5 x 10^6 cells	4	nd
	1.Experiment	5,7 x 10^6 cells	7	76.5
	2.Experiment	14 x 10^6 cells	11	79,4

2.1.2. Cell Line OMM-1

This cell line was isolated from the skin metastasis of a 74-year-old man diagnosed with uveal melanoma. The primary neoplasm had been diagnosed 29 years earlier and was successfully treated by enucleation (Luyten et al. 1996:381). As the literature indicates, the

karyogram of this cell line shows an approximately triploid chromosome set (Luyten et al. 1996:385), a suspected monosomy of the third chromosome could be excluded by White et al. (2006:16). Confirmation of mutation in gene GNA11 as well as expression of protein BAP1 was performed by Amirouchene-Angelozzi et al. (2014:1512).

For the experiment we thawed 5 x 10^6 Cells with a passage of 5 and transferred them into a T75 flask. Luyten et al. (1996:381) described the cell line as a mixture of adherent and non-adherent cells, with adherent cells becoming increasingly apparent as the passage progressed. In figure 3A, a bean-shaped aggregate of cells can be viewed centrally. The spherical non-adherent cells of this cell line increasingly collect (see figure 3B), whereas in figure 3C the adherent cells with their extensions can also be observed. In figure 3D at 400x magnification, the predominantly spindle cell-like structure of the cells can be seen, the cell nuclei are well delineated and the nucleoli appear prominent. Amirouchene-Angelozzi et al. (2014:1512) describes a doubling time of 34 h for the cell line OMM-1. In routine cell culture, we split the cells 1:3 every two days on average depending on the confluence.

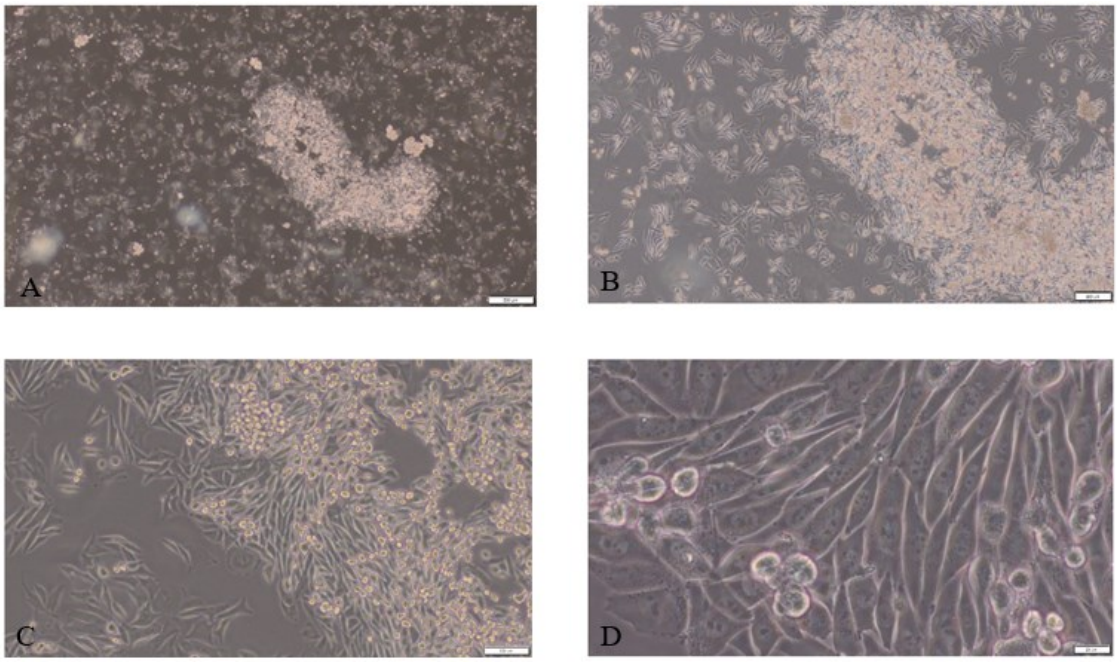

Figure 3. Cell line OMM-1, passage 6, (A) 20x magnification, (B) 40x magnification, (C) 100x magnification, (D) 400x magnification, scale bar: 20µm.

For the first experiment, we were able to grow 13x10^6 Cells, p7 with a viability of 57,1%. During routine cell culture, this cell line was eliminated for the second experiment due to bacterial contamination.

Table 3 shows the cell numbers, passage and viability at respective measuring points.

Table 3. *Cell count, passage and viability of the cell line OMM-1 in relation to the different measuring points. nd =not determined. - = excluded from experiment.*

OMM-1	Measuring points	Cell count	Passage	Viability in %
	Thawing	5 x 10^6 cells	5	nd
	1.Experiment	13 x 10^6 cells	7	57.1
	2.Experiment	-	-	-

2.1.3. Cell Line Mel270

Jager et al. (2016:6) describes in detail the timeline of this patient's history. The Mel270 cell line was 1994 isolated from the uveal melanoma of a 79-year-old man. 17 years earlier, a nevus in his right eye was documented as an incidental finding in the course of disease of his left eye. This nevus was regularly checked and observed for morphologic changes. Ten years later this nevus developed into a choroidal melanoma which was treated with an iodine-125 plaque. The patient was in remission until 1994, but suffered from hemorrhages caused by the radiation of the treatment which consequently reduced his visual acuity to light perception. During the year, a progression in the growth of the uveal melanoma was also confirmed as the tumor grew in height from 2,5 mm to 12,7 mm but did not infiltrate adjacent structures. Shortly thereafter, enucleation of the right eye was performed in 1994, whereby the brownish pigmented tumor was removed and made available for cell line isolation. After histological processing of the tumor tissue, the microscope showed pleomorphic cells in the tumor. In addition to spindle-shaped cells with elongated nuclei and prominent nucleoli, epithelioid cells were also detected (Jager et al. 2016:6). A year later, the patient was diagnosed with several liver metastases as well as bone metastases.

For our experiment, 5 x 10^6 Cells, p5 were thawed and then transferred to a T75 flask. In routine cell culture, morphologically, the adherent cell line is most notable for its spindle-shaped cells (see figure 4A), some of which fork into two extensions at the respective poles (see figure 4B). The nucleoli can be distinguished from the rest of the cell. No doubling time could be determined from the literature, however in the laboratory we split the cells on average 1:4.5 every 2 days. Concerning the genetic alterations, a monosomy of the third chromosome could be disproved by White et al. (2006:16) while a tetrasomy 6p and a disomy 8q were noted (Jager et al. 2006). The GNAQ mutation which is typical for uveal melanomas was described by Griewank et al. (2012:184). BAP1 expression was identified by Jager et al. (2016:4).

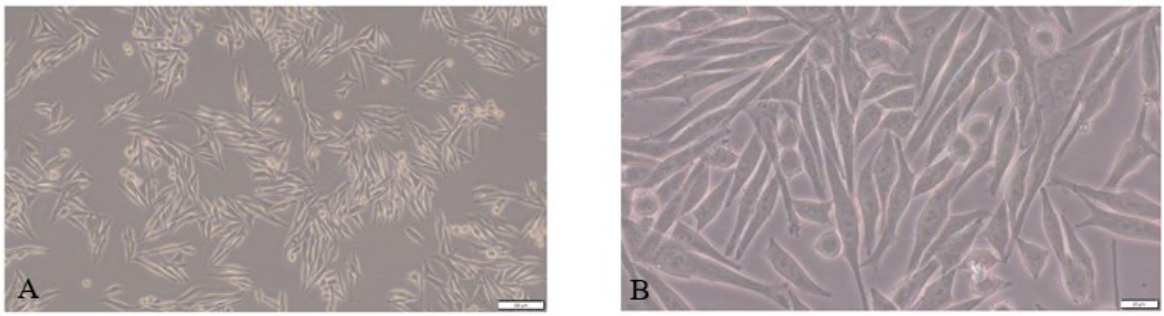

Figure 4. Cell line Mel270, passage 6, (A) 100x magnification, (B) 400x magnification, scale bar: 20µm.

For the first experiment 29,9x10^6 Cells, p7 with a viability of 86,1% were grown while for the second experiment 9x10^6 Cells, p10 with a viability of 95,1% were gathered. Table 4 shows the cell numbers, passage and viability at respective measuring points.

Table 4. *Cell count, passage and viability of the cell line Mel270 in relation to the different measuring points. nd =not determined*

Mel270	Measuring points	Cell count	Passage	Viability in %
	Thawing	5 x 10^6 cells	5	nd
	1.Experiment	29,9 x 10^6 cells	7	86.1
	2.Experiment	9 x 10^6 cells	10	95.1

2.1.4. Cell Line OMM-2.3

This cell line was acquired from the liver metastasis of the same patient whose primary tumor was utilized for the Mel270 cell line. It took 8 years from the diagnosis of the primary tumor to the appearance of the metastases. After surgical removal, the patient received chemotherapy but died shortly afterwards (Jager et al. 2016:6).

For our experiments we transferred 1 x 10^6 cells into a T75 flask. Under the microscope, this cell line showed adherence. The cell type is mixed, with spindle-shaped cells as well as polygonal cells visible (see figure 5A). On closer inspection, the lighter nuclei are clearly distinguishable from the darker nucleoli, see figure 5B. For this specific cell line no doubling time could be found in the literature, but for the cell line OMM-2.5, which also represents a liver metastasis of the same primary tumor and could possibly provide a reference, the doubling time was found to be 50 h (Amirouchene-Angelozzi et al. 2014:1512). In routine cell culture, we split cells depending on confluence at an average of 1:4,5 every 3 days.

Genetic studies also showed a disomy of the 3rd chromosome (White et al. 2006:16) in the presence of a GNAQ mutation (Griewank et al. 2012:184) and the absence of a BAP1 mutation (Jager et al. 2016:12).

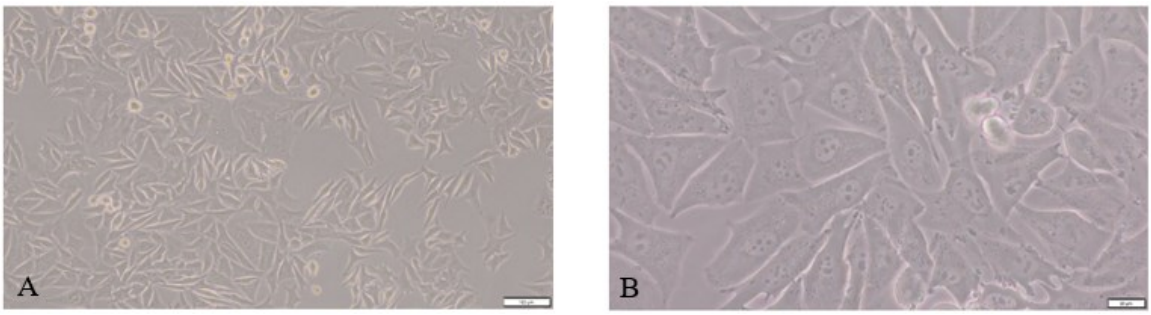

Figure 5. Cell line OMM-2.3, passage 24, (A) 100x magnification, (B) 400x magnification, scale bar: 20µm.

During the laboratory work, the indication of a possible cross-contamination occurred, whereupon all flasks of this cell line were discarded and therefore 1 x 10^6 cells were thawed. For the first experiment 5,8 x 10^6 cells , p26 and a viability of 67.1% was obtained while for the second experiment 9 x 10^6 cells were counted. Table 5 shows the cell numbers, passage and viability at respective measuring points.

Table 5. *Cell count, passage and viability of the cell line OMM-2.3 in relation to the different measuring points. nd =not determined*

OMM-2.3	Measuring points	Cell count	Passage	Viability in %
	Thawing	1 x 10^6 cells	24	nd
	1.Experiment	5,8 x 10^6 cells	26	67.1
	Thawing (second time)	1 x 10^6 cells	24	nd
	2.Experiment	9 x 10^6 cells	27	87.2

2.2. Preparation of the CAM

In advance, 110 white fertilized Lohmann eggs were ordered (Schropper GmbH, A-2640 Gloggnitz, Auestraße 35, T: +43 (0) 2663/8305-9, F:+43 (0) 2663/8305-10, w: www.schropper.at).

When the eggs arrived they were washed under running lukewarm water and cleaned with a toothbrush to get rid of the visible stains. After they dried, the eggs were sprayed with 70% EtOH to further reduce the risk of contamination. Afterwards they were gently distributed onto the broodroll hordes and put into the incubator (J. Hemel Incubators Easy series) in a horizontal position as illustrated in figure 6. It is also important to notice that the broodroll

hordes were fixated with a metal plate and butterfly nut. This arrangement was chosen because the eggs are slightly cradled during their incubation period, thus reducing the risk of injury to the eggs. In addition, the incubator contains two tanks filled with aqua bidest to keep the humidity in the incubator on a constant level. Eventually the eggs were incubated at a temperature of 37.6°C. The condition of the eggs was controlled regularly and dead or contaminated eggs were sorted out on a daily basis.

Figure 6. Horizontal placement of the eggs on the brood roll hordes in the incubator. The brood roll hordes were fixated with a metal plate to ensure slight movement of the eggs. The black water tanks can be seen below.

2.2.1. Ex Ovo Cultivation: Cracking Process

On the third day of incubation the eggs are suitable for cracking. During this process, it is important that the eggs are not turned over and that they always remain in the exact horizontal position in which they were placed in the incubator.

An egg was taken and the underside was dipped about 2cm into a container of 70% EtOH. After drying, the shell of the egg was carefully cut with an electric blade in three positions. These specific breaking points were chosen because they pose the lowest risk of damaging the yolk while at the same time freeing the egg from the shell as effectively as possible. Now, index fingers are gently placed on the egg, and the thumb and middle fingers are used to grasp the egg on both sides and briefly press it lightly into the scales pan. It is important that the index fingers do not exert pressure on the egg from above. After a cracking sound, the two index fingers are pressed against each other so that the thumbs can open the egg with light pressure. Now the cracked eggs were closed with a lid to avoid contamination and placed on the tray for further incubation at 37.6°C and 40-60% humidity. The most important steps of the cracking process can be seen in figure 7 A-D. For the first experiment twelve eggs and for the second experiment 16 eggs were selected. The remaining eggs were used for different experiments.

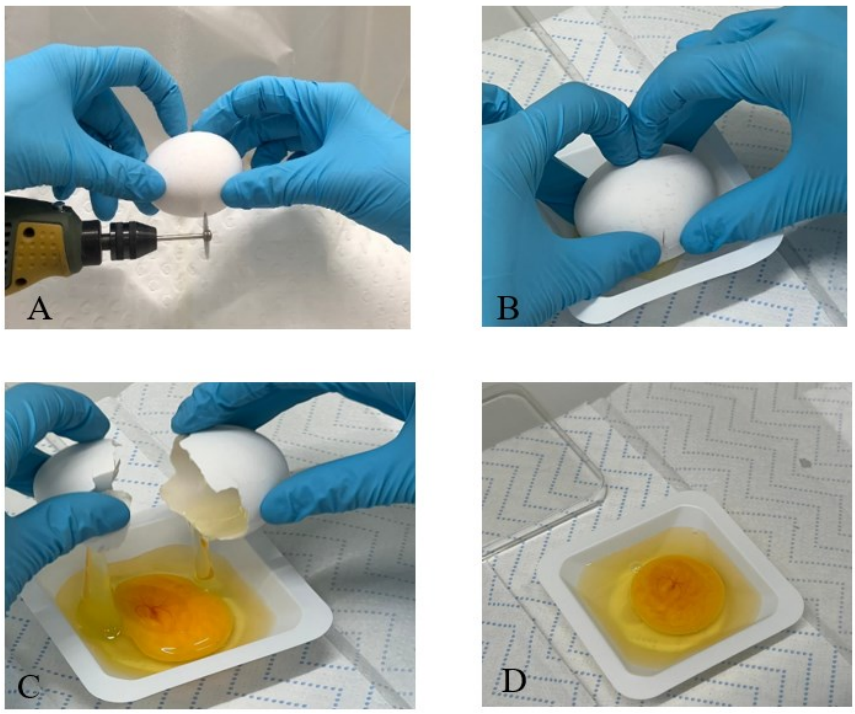

Figure 7. Cracking process. (A) Cutting the shell of the egg with an electric blade. (B) Opening process of the egg, both fingers exert pressure against each other. (C) Gently opening the egg. (D) The cracked egg, next to it the lid.

2.3. Testing Matrix for Uveal Melanoma Cell Lines

The choice of the right matrix for respective cells is crucial, as the different formulations of the matrices have an influence on cell proliferation. Enriched with proteins and growth factors, the matrix should provide the most physiological and growth-promoting environment possible for the cells in the same way as an extracellular substance (Hughes et al., 2010:1886-1890). Three different matrices were tested for this study: Matrigel®, Geltrex™ and pure cell culture medium. Each cell line was spiked with each matrix condition. The onplants were transplanted onto the CAM on day ten. Only eggs with developmentally appropriate vascularisation and a well-moving embryo were used. Eggs that showed a grey haze or signs of contamination were discarded.

For the experiment, a master mix consisting of 15µl cell suspension and 5µl matrix each was first prepared. For the cell suspension, the cells were resuspended with PBS. A concentration of $1x10^6$ cells/15 µl was used for the cell lines OMM-1 and Mel270 and a concentration of $0.5\ x10^6$ cells/15 µl for the cell lines 92.1 and OMM-2.3. The total volume for one onplant was 20µl, as shown in table 6.

Table 6. *Composition of the master mix. The rows show the cell lines depending on the number of cells used per onplants. Each row represents a cell line, with cell line 92.1 showing a lilac background colour, cell line OMM-2.3 a yellow background colour, cell line OMM-1 a pink background colour and cell line Mel270 an orange background colour. The columns reflect the matrix conditions. The medium condition is striped red, no additives other than PBS and the cell medium RPMI1640 were used. The Matrigel® condition is striped blue. The Geltrex™ condition is striped green. The total volume is 20µl/ onplant consisting of 15µl cell suspension and 5µl matrix.*

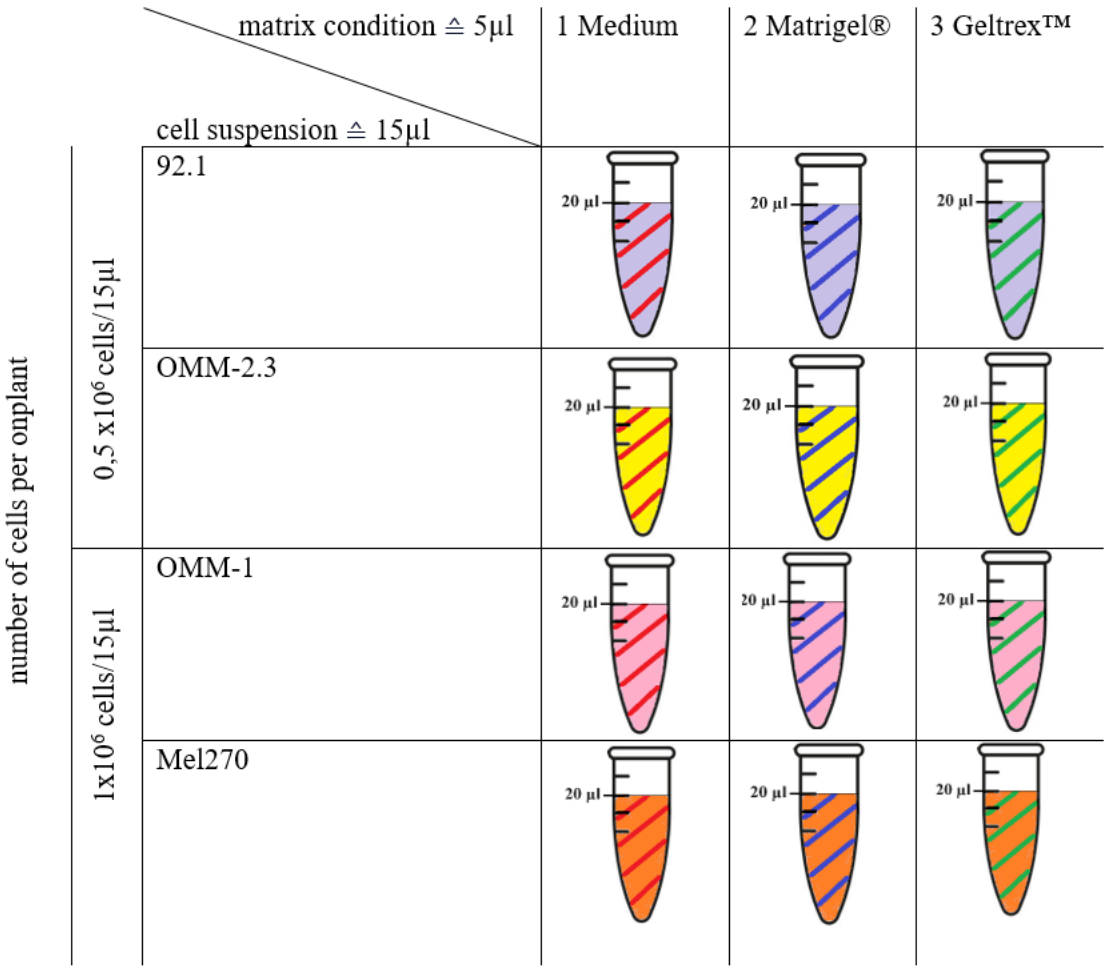

Parallel to the preparation of the master mixes, three autoclaved silicone rings were placed on each egg to localise the onplants. The silicone rings were placed on the CAM taking into account the further expansion of the CAM and at a certain distance from the pulsating arteries and the other silicone rings. The master mix, cooled on ice, was then applied to the silicone rings at 20µl each using a calibrated pipette and frozen pipette tips according to the scheme in table 7. The onplants and CAM were then incubated for a further four days at 37.6°C and 40-60% humidity.

Table 7. *Scheme of the application of the master mix, first experiment eggs #129-140. Each row represents a cell line, with cell line 92.1 showing a lilac background colour, cell line OMM-2.3 a yellow background colour, cell line OMM-1 a pink background colour and cell line Mel270 an orange background colour. Each square represents an egg, the circles in the squares reflect the onplants (n=36) with their matrix conditions. Onplants with number 1 are striped red, no other additives besides PBS and cell culture medium were used. Onplants with number 2 are striped blue, Matrigel® was used as matrix condition. Onplants with number 3 are striped green, Geltrex™ was used as matrix condition. A total of three onplants were available for investigation for each cell line, depending on the matrix condition.*

cell line			
92.1 Eggs #129-131	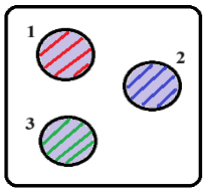	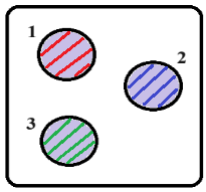	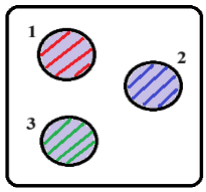
OMM-2.3 Eggs #132-134	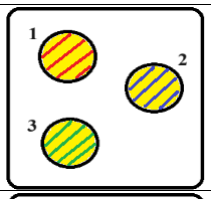	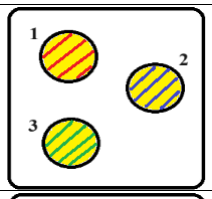	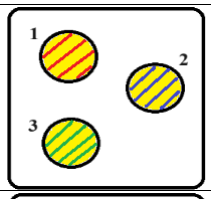
OMM-1 Eggs #135-137	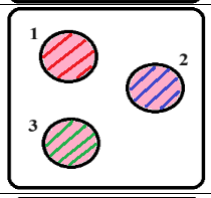	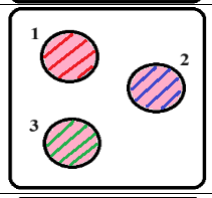	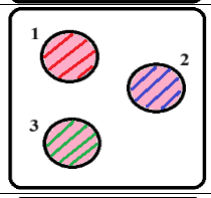
Mel270 Eggs# 138-140	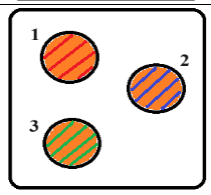	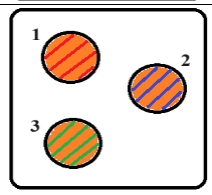	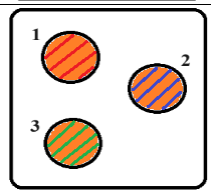

2.4. Testing Potential Drug Melphalan

The second experiment deals with the potential active ingredient Melphalan and was carried out after the first experiment. The procedure for transplanting the cells was analogous to the first experiment, with minor deviations that are explained below. The cell line OMM-1 was excluded from this experiment due to contamination.

2.4.1. Transferring the Cell Lines on the CAM

The cells were transplanted on the ninth day. For this purpose, a master mix consisting of 15µl cell suspension with a concentration of $1x10^6$ cells/15µl and 5µl Matrigel® was prepared for all cell lines. The onplants with the cell line 92.1 comprised a volume of 20µl, for the cell lines Mel270 and OMM-2.3 a volume of 18µl/ onplant was obtained due to

human factors. A total of 16 eggs were used, on each of which two to three onplants were planted, see table 8.

Table 8. *Scheme of the application of the master mix, second experiment eggs #141-156. Each row represents a cell line, with cell line 92.1 showing a lilac background colour, cell line OMM-2.3 a yellow background colour and cell line Mel270 an orange background colour. Each square represents an egg, the circles in the squares reflect the numbered onplants (n=37). The blue stripes represent the used matrix Matrige®l. Melphalan was applied to onplants marked with a red dot. Melphalan was not applied to egg #153 due to contamination on the tenth day.*

cell line				
92.1 Eggs #141-144	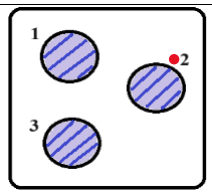	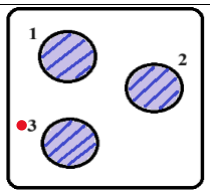	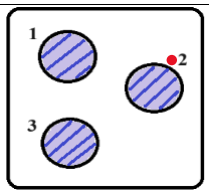	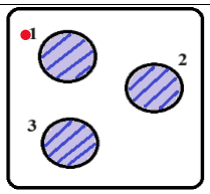
OMM-2.3 Eggs #145-148	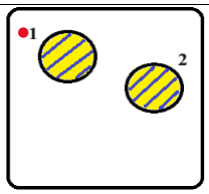	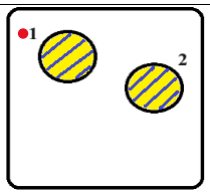	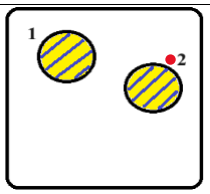	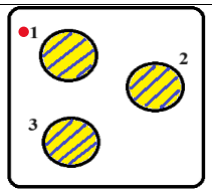
Mel270 Eggs #149-152	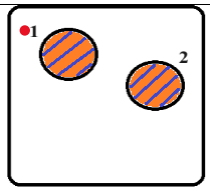	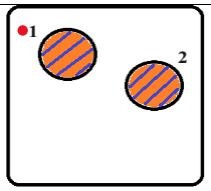	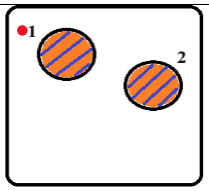	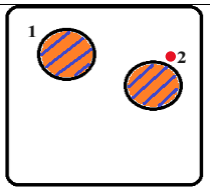
Eggs #153-156	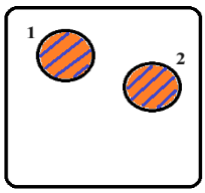	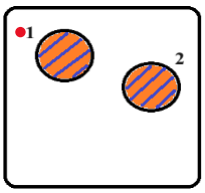	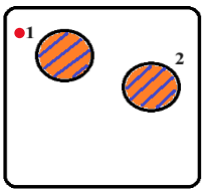	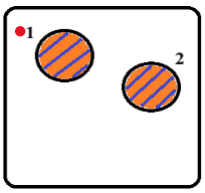

2.4.2. Dosing and Application of Melphalan

Melphalan (Melphalan Tillomed 50mg, with a concentration of 5mg/ml, batch designation: MHAA22003C) was kindly provided by the Anstaltsapotheke des Landeskrankenhauses - Universitätsklinikum Graz. On the day of receipt, Melphalan was portioned directly under the Laminar Flow Cabinet (Thermo Scientific HERASAFE KS) in seven sterile Eppendorf tubes of 1ml each and frozen at -20°C. On the tenth day post-fertilisation, an Eppendorf tube containing 1ml was thawed. The drug was then diluted with PBS to a concentration of 10µl/ml and applied to the respective onplants (see table 8, red dots). The amount of active ingredient used was calculated with the help of the comprehensive study by Munier et al (2019:2-56). The drug was applied to the macroscopically largest tumours as follows. First, 10µl were applied to the respective tumours, then the chick embryos were placed in the

incubator at 37.6°C and 40-60% humidity for ten minutes. Melphalan was then washed five times with 10µl RPMI-1640 medium with L-glutamine using a calibrated pipette. The eggs were then returned to the incubator at 37.6°C and 40-60% humidity for a further 72 hours.

2.5. Harvest, Fixation and Paraffin Embedding

The xenografts were excised on day 14 of the first experiment and day 13 of the second experiment. First, the chick embryos were placed on ice to sedate them, then the xenografts were photodocumented using a microscope (Olympus SZX15) and the cellSens software. While working with the xenografts it important to wear gloves at all times to ensure RNAse free condition. Using a medical scissor and tweezers, the xenograft and silicone ring were cut out, transferred to PBS and photographed again. The xenografts were then placed in 4%PFA to stop the denaturation of proteins and thus fix the tissue. This fixation process takes 24 hours and is carried out at room temperature using a labelled, sealed plastic dish.

The following day, the xenografts were each placed in a Tissue-Tek embedding casette, surrounded on both sides by suitably sized paper rectangles, to prepare them for subsequent alcohol series and paraffin embedding (see table 9).

Table 9. *Alcohol series and paraffin embedding protocol.*

Reagents	Duration / Temperature
70% EtOH	30 min/ RT
95% EtOH	30 min/RT
95% EtOH	15 min/RT
100% EtOH	30 min/RT
100% EtOH	15 min/RT
Toluene	30 min/RT
Toluene	15 min/RT
Infiltration with paraffin #6	30 min/62°C
Infiltration with paraffin #6	30 min/62°C
Embedding in paraffin #6	62°C

For the last step of the protocol, the two pieces of paper and the silicone rings were first removed with tweezers. The silicone rings were then collected in a metal box for cleaning and reuse. In order to transfer the xenografts into paraffin blocks, a narrow bottom cover of paraffin #6 was poured into the preheated metal moulds. The xenografts were quickly placed

vertically in the centre and the rest of the metal mould was filled with paraffin #6 using the paraffin dispenser (Kunz instruments Paraffin Dispenser WD-4). Finally, the labelled plastic cassette was also placed in the metal mould. The still warm paraffin block was then placed on a cooling plate (Microm AP280-1) at -9°C to harden. The finished paraffin blocks were then removed from their metal mould and stored at 4°C in a dust- and shatterproof place.

2.6. Microtomy

Before the paraffin blocks could be cut, they were examined for cracks. Suitable blocks were then cut with a sharp razor blade, leaving an approximately 1cm x 1cm block of paraffin with the xenograft. The paraffin block was then clamped in the microtome (Leica RM2245 V2.4 rotary microtome, Leica Biosystems Nussloch GmbH) and 5µm thin sections were made. Two brushes were used as support, with which the sections were transferred to a aqua bidest bath at room temperature. Chrome alum-gelatine object slides were dipped into the same container to centre the sections on the slide. The slide was then slowly immersed in an aqua bidest bath (GFL Typ 1052) heated to 45°C. The sections, slightly curled by the microtome, flattened under the influence of the warm liquid and were then placed on a heating plate (Medite OTS 40) at 41.5°C for three hours to bake out. The main work steps are illustrated in figure 8.

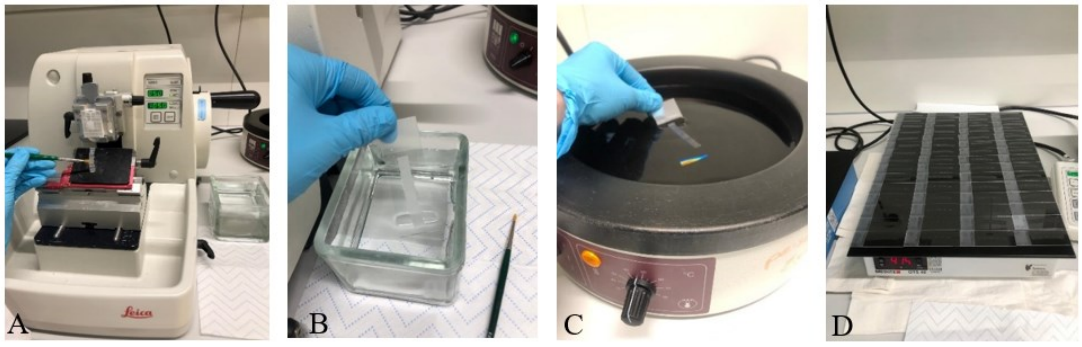

Figure 8. Working steps from the paraffin block to the microscope slide. (A) The microtome with the clamped paraffin block. A 5µm thin paraffin section is created by repeatedly turning the crank. (B) Immersing the slide in aqua bidest to centre the paraffin section. (C) Immersing the slide in a 45°C water bath. (D) Heating plate and arrangement of the slides.

2.7 Tissue Staining

All sections from both experiments were stained with hematoxylin-eosin staining for comparison. Immunohistochemistry staining was used for the second experiment, with one section stained for each cell line from each group (treated vs. control) to provide a reference for later experiments.

2.7.1 Hematoxylin and Eosin Staining

Hematoxylin and eosin staining is one of the most important routine stains in histology and is used to systematically stain tissue so that different cells and structures can be easily distinguished from one another. The staining was carried out using the protocol shown in table 10 which is described in more detail in the following. As the sections are embedded in non-water-soluble paraffin, the first step serves to deparaffinise them. This is ensured by the first two steps with xylene. A descending alcohol series then follows, which is intended to rehydrate the tissue first. Starting with 100% EtOH, which is supposed to remove the xylene and finishing with 50% EtOH. The alcohol series is followed by two minutes in aqua bidest with the aim of rehydrating the tissue. Subsequently the slides are stained with hematoxylin (hemalum solution acid acc. to Mayer, ROTH) for 90 seconds, binding to basophilic structures like cell nuclei, ribosomes and DNA. Rinsing the slides with tap water for 15 minutes changes the pH value to alkaline and causes a colour change from wine red to blue-violet. The slides are then briefly dipped in aqua bidest and immersed in eosin for six seconds. The eosin dye colours predominantly alkaline cell structures, such as cytoplasm and proteins, intensely pink to pale pink. After a one-minute dwell in aqua bidest, an ascending alcohol series was performed to dehydrate the sections. It was initiated by an 80% EtOH solution, followed by 95% and 100%. Finally, the slides are immersed in Xylene to clarify them and dripped with inclusion agent (Roti ® Histokitt II) before being covered with cover slips for protection (Welsch et al., 2022:7-10). After approximately one day, the sections are completely dry and ready for microscopy.

Table 10. *Protocol for hematoxylin and eosin staining*

Reagents	Duration	Info
Xylene	2 min	Deparaffinization
Xylene	2 min	
100% EtOH	2 min	Removal of xylene and rehydration
100% EtOH	2 min	
95% EtOH	2 min	
80% EtOH	2 min	
50% EtOH	2 min	
Aqua bidest	2 min	
Aqua bidest	2 min	
Hematoxylin	1 min 30 seconds	Nuclear staining and bluing
Tap water	15 min	
Aqua bidest	Dip	
Eosin	6 seconds	Counterstaining
Aqua bidest	1 min	
80%	1 min	Dehydration
95%	1 min	
100%	1 min	
100%	1 min	
Xylene	1 min	Clearing
Xylene	1 min	
Xylene	1 min	

2.7.1 Immunhistochemistry Staining: Ki-67 and CK

The immunohistochemical staining serves as a preliminary overview and is intended to provide initial indications for all subsequent experiments. The proliferation index Ki-67 and pancytokeratin (CK) staining are analysed. Ki-67 is a protein that is present in the cell nucleus during the interphase of the cell cycle. During mitosis, the cell nucleus dissolves and Ki-67 can be immunohistochemically stained with the help of an antibody and thus mark all cells that are in proliferation (Sun and Kaufman, 2018:1-2). In this study, Ki-67 positive cells are stained blue instead of the usual brown, as the uveal melanoma cells themselves are partially brown pigmented and a reliable evaluation is otherwise not possible. In order to

describe potential differences in proliferation between the treated and untreated tumours, the number of positive cells in the untreated tumours was compared with the number of positive cells in the treated tumours. Three high-power fields (400x magnification) were used, which were randomly inserted into a grid as shown in figure 9 and counted manually. The cytokeratin staining marks the CAM epithelia royal blue so that invasive growth into the CAM epithelium can be visualised and analysed.

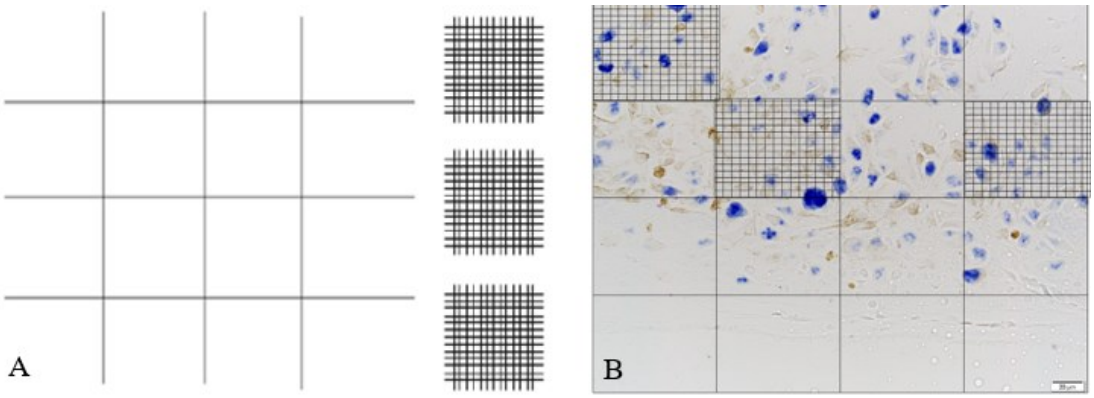

Figure 9. Manual counting of the Ki-67 positive cells. (A) The grid with the three high-power fields. (B) Ki-67 staining at 400x magnification with the grid and the three randomly assigned high-power fields. Scale bar 20 µm.

3. Results

3.1. Testing Matrix for Uveal Melanoma Cell Lines

3.1.1. Macroscopic Tumour Formation

The four uveal melanoma cell lines grew differently on the CAM and formed macroscopically varying tumours. What they have in common is that each cell line, in combination with the Matrigel® matrix used, formed the largest macroscopic tumours. The most promising tumours were obtained with cell line 92.1. The tumours of this cell line appear with Matrigel® as a brownish nodule with radial vessel formation; no tumour growth could be shown macroscopically for the matrix condition Medium or Geltrex™ (see figure 10). Cell line OMM-2.3 combining with Matrigel® shows a white, regular and sharply defined tumour with radial sprouting vessels, whereby no tumour growth could be observed macroscopically when using Medium or Geltrex™ (see fig. 13 1-3A). The cell line OMM-1 formed irregularly bordered white tumours with Matrigel®, whereas no tumour growth was observed with Medium or Geltrex™ (see fig. 14 1-3A). The Mel270 cell line generally grew the poorest on the CAM. In the Matrigel® condition, a discrete whitish nodule with increased perinodular vascularisation was observed, while in the other two conditions there was again no tumour growth (see fig. 15 1-3A).

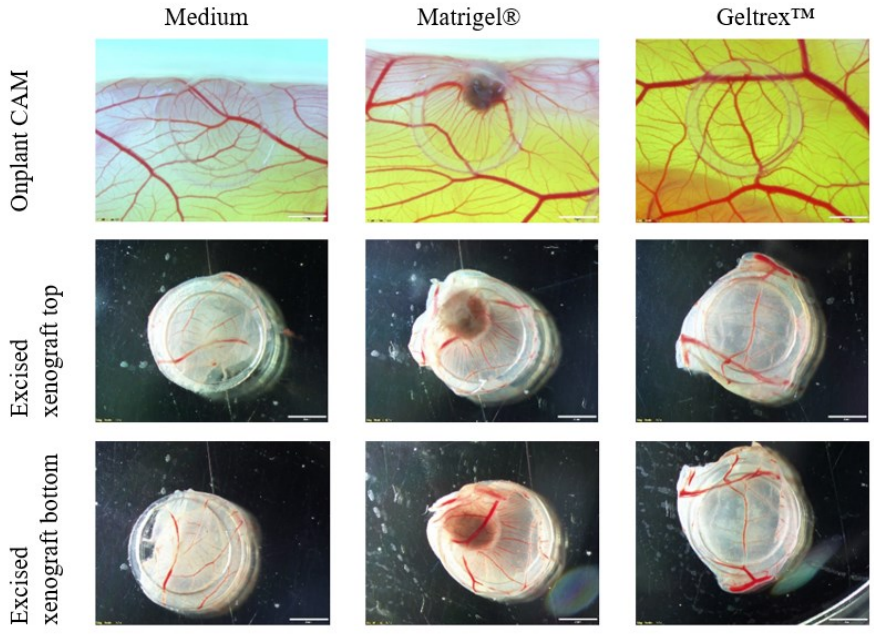

Figure 10. Macroscopic overview of the CAM tumours of cell line 92.1 depending on the matrix condition. Under the influence of Matrigel®, a brownish nodule with radial vascularisation develops. No macroscopic tumour growth could be shown in the Medium or Geltrex™ condition. The photos shown are exemplary for the onplants on the CAM and the excised xenografts. Scale bar 2mm.

3.1.2. Histological Analysis

To describe the microscopic tumour morphology, sections with hematoxylin-eosin staining were used for overview purposes. The xenograft consists of the following most important components, which are depicted in figure 14. The CAM is marked with black arrows. It has an upper and lower epithelium, which is connected by vascularised mesenchyme. The uveal melanoma tumour, here exemplified by cell line 92.1 influenced by Matrigel®, is shown with a blue arrow. The vessels of the tumour are marked with red arrows. In this example, the tumour is infiltrated by Matrigel®, shown with green arrows.

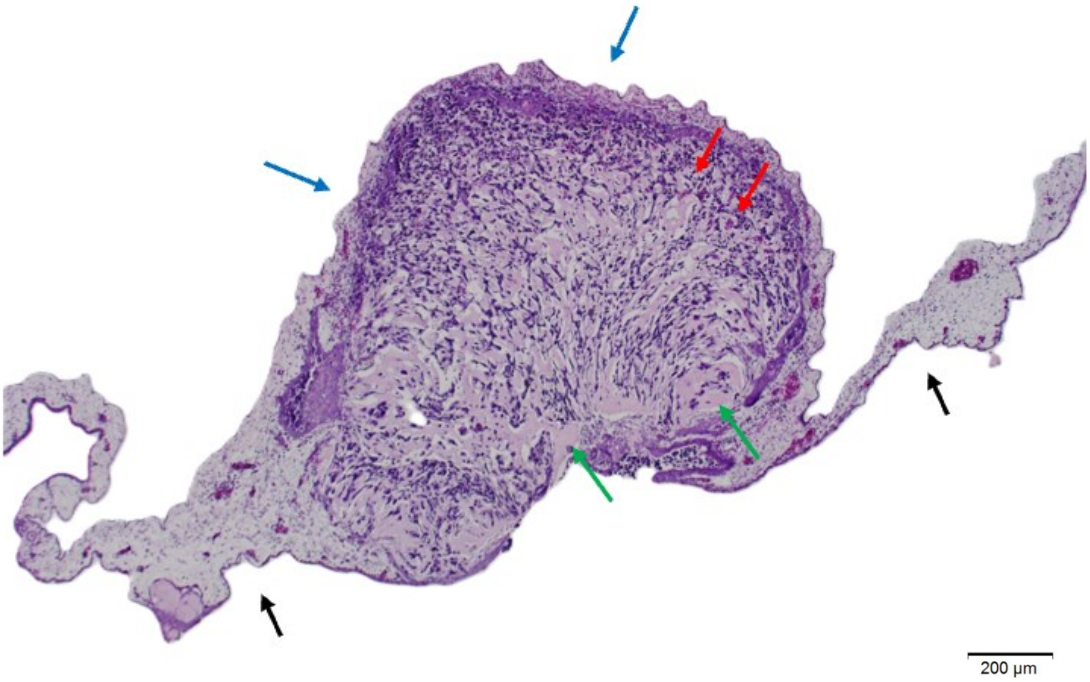

Figure 11. Xenograft of the cell line 92.1 at 40x magnification using hematoxylin eosin staining. Black arrows point to the CAM. Blue arrows show the tumour with its vessels (red arrows) and Matrigel® (green arrows). Scale bar 200µm.

The following figures 12-15 show the tumours of the cell lines depending on the matrix condition. To provide an overview, the onplant was first shown on the CAM immediately before excision. The hematoxylin-eosin staining was photographed in 40x, 100x, 200x and 400x magnification.

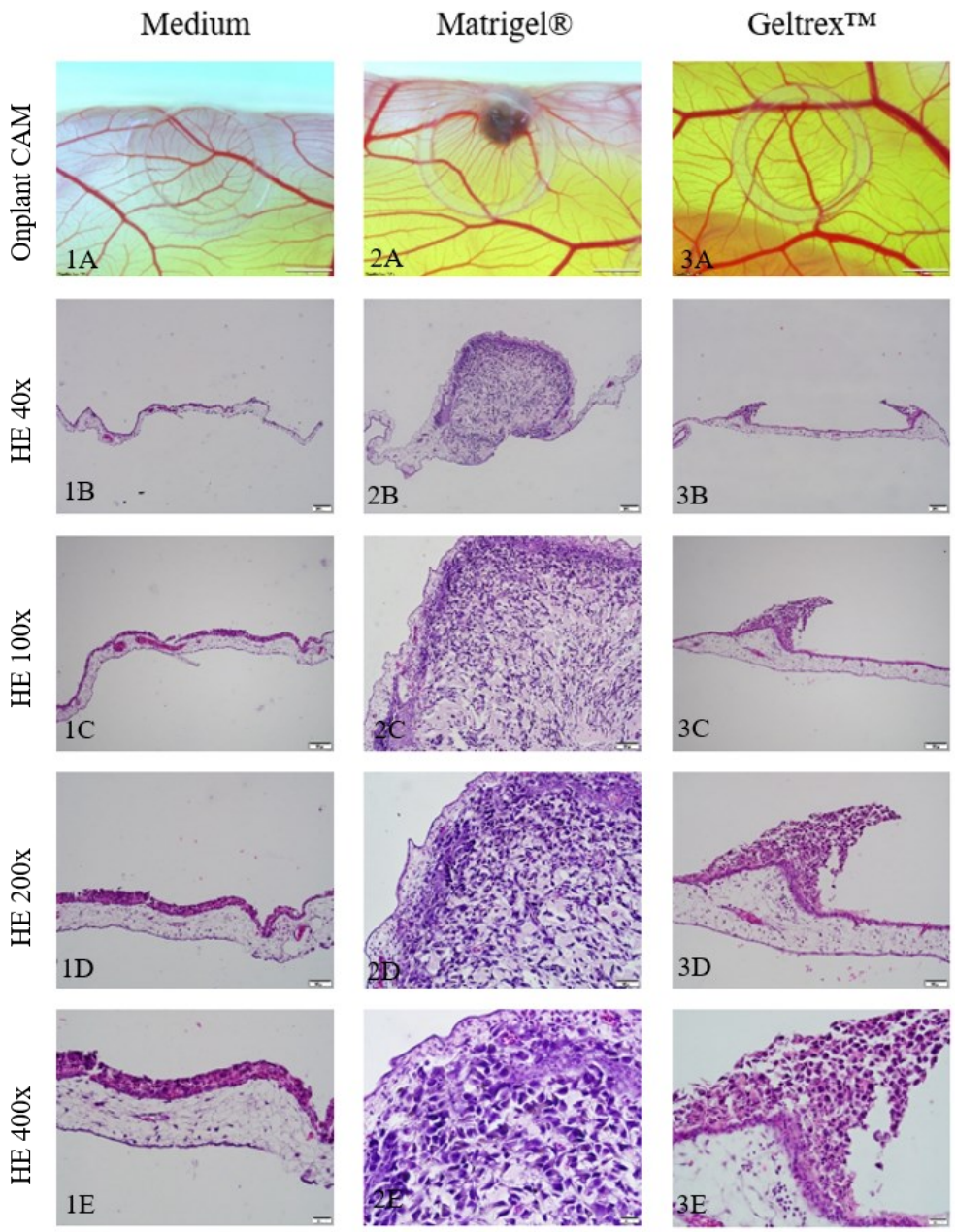

Figure 12. CAM tumour histology of cell line 92.1 depending on the matrix condition. One of the three matrix conditions is illustrated for each column. Images of the onplant on the CAM labelled (1A)-(3A) serve as an overview for the following HE stains, scale bar: 2mm. The HE stains were photographed at 40x, 100x, 200x and 400x magnification. Scale bar (1B)- (3B): 200µm, (1C)- (3C): 100µm, (1D)- (3D): 50µm, (1E)- (3E): 20 µm.

(1A)-(1E) The xenograft grown under the influence of medium. In these images, a thin fringe of polymorphic tumour cells with several prominent nucleoli and immigration of immature chicken erythrocytes (normoblasts) into basal sections of the cell fringe can be observed. (2A)- (2E) The xenograft grown under the influence of Matrigel® which depicts infiltrative growth of tumour cells with partly spindle-shaped to multipolar cell bodies, melanocytic pigment inclusions and reticular infiltration of Matrigel® throughout the tumour. (3A)-(3E) The xenograft grown under the influence of Geltrex™. The tumour cells are in loose association and show a polymorphous cell pattern with pyknotic nuclei. There is no invasive growth detectable.

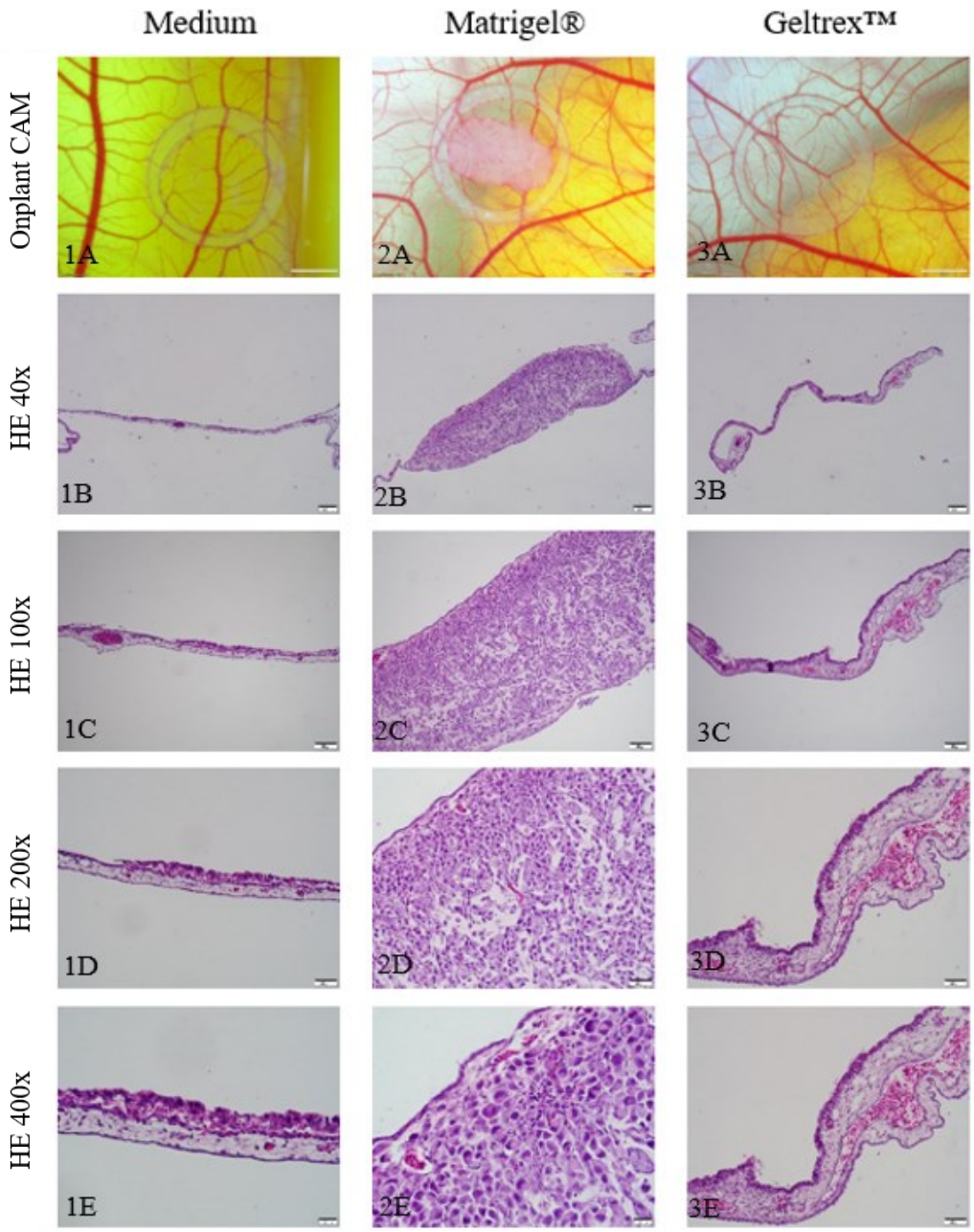

Figure 13. CAM tumour histology of cell line OMM-2.3 depending on the matrix condition. One of the three matrix conditions is illustrated for each column. Images of the onplant on the CAM labelled (1A)-(3A) serve as an overview for the following HE stains, scale bar: 2mm. The HE stains were photographed at 40x, 100x, 200x and 400x magnification. Scale bar (1B)- (3B): 200µm, (1C)- (3C): 100µm, (1D)- (3D): 50µm, (1E)- (3E): 20 µm.

(1A)-(1E) The xenograft grown under the influence of medium. In these images, a discontinuous narrow fringe of polymorphous tumour cells can be observed. There is no infiltrative growth into the CAM epithelium. (2A)-(2E) The xenograft grown under the influence of Matrigel® which depicts infiltrative growth of tumour cells with round tumour cell bodies and crescent-shaped, partly binucleated nuclei that vary in orientation. (3A)-(3E) The xenograft grown under the influence of Geltrex™. This tumour shows a dense narrow fringe of tumour cells with no invasive growth into the CAM epithelium.

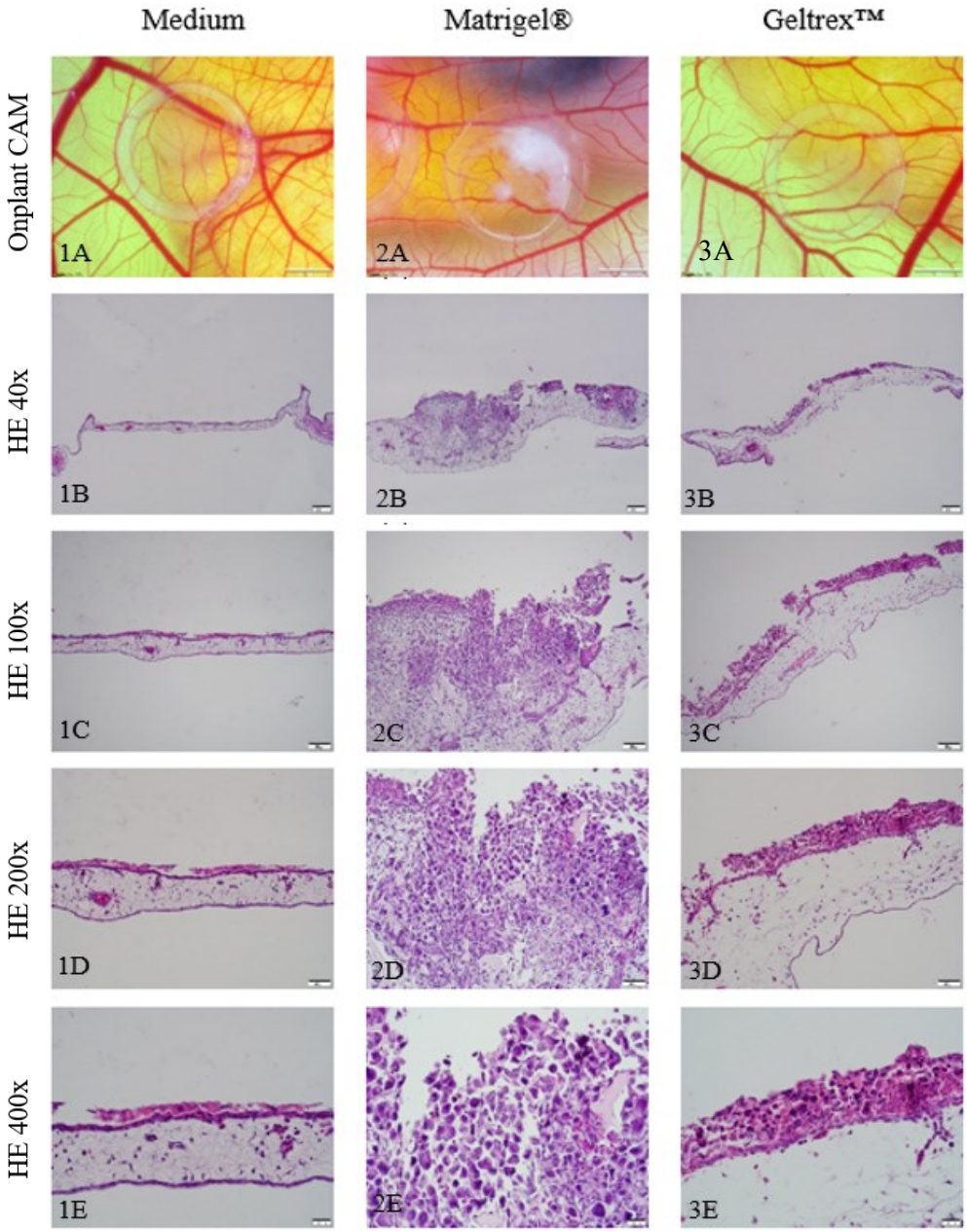

Figure 14. CAM tumour histology of cell line OMM-1 depending on the matrix condition. One of the three matrix conditions is illustrated for each column. Images of the onplant on the CAM labelled (1A)-(3A) serve as an overview for the following HE stains, scale bar: 2mm. The HE stains were photographed at 40x, 100x, 200x and 400x magnification. Scale bar (1B)- (3B): 200µm, (1C)- (3C): 100µm, (1D)- (3D): 50µm, (1E)- (3E): 20 µm.

(1A)-(1E)The xenograft grown under the influence of medium. In these images, a discontinuous narrow fringe of tumour mass with blurred cell boundaries is illustrated. There is no invasive growth into the CAM epithelium. (2A)-(2E) The xenograft grown under the influence of Matrigel® which depicts infiltrative growth of polymorphous tumour cells with pathological nucleus-plasma ratio, pyknotic nuclei and partly spindle-shaped cell bodys. In the center are remains of Matrigel®. (3A)-(3E) The xenograft grown under the influence of Geltrex™. This tumour shows a loosened cell cluster with polymorphous partly pyknotic tumour cells and nuclei with sporadicallly mitotic figures.

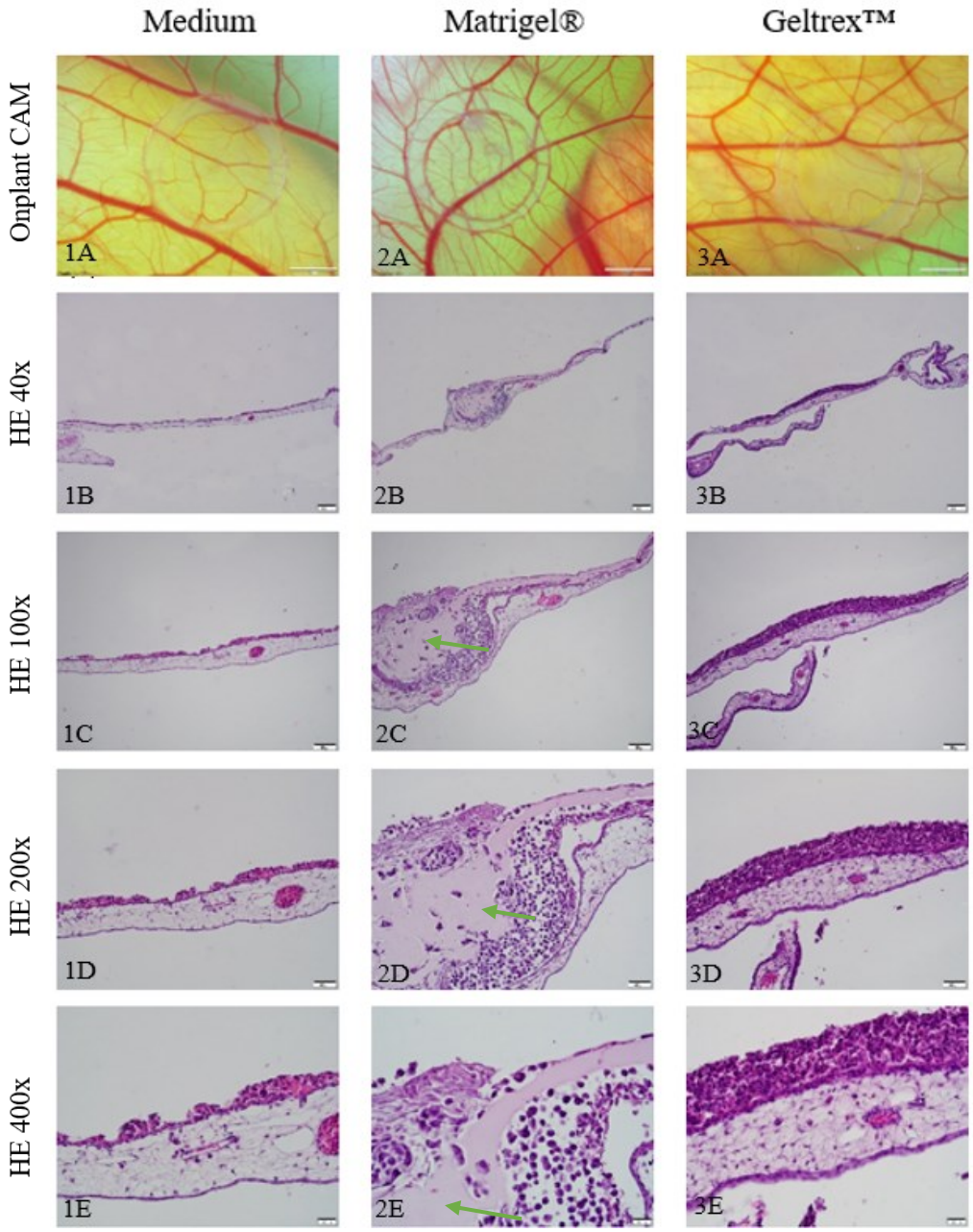

Figure 15. CAM tumour histology of cell line Mel270 depending on the matrix condition. One of the three matrix conditions is illustrated for each column. Images of the onplant on the CAM labelled (1A)-(3A) serve as an overview for the following HE stains, scale bar: 2mm. The HE stains were photographed at 40x, 100x, 200x and 400x magnification. Scale bar (1B)- (3B): 200µm, (1C)- (3C): 100µm, (1D)- (3D): 50µm, (1E)- (3E): 20 µm.

(1A)-(1E) The xenograft grown under the influence of medium. In these images, a discontinuous narrow fringe of polymorphous tumour cells is illustrated. There is no invasive growth into the CAM epithelium. (2A)-(2E) The xenograft grown under the influence of Matrigel® which depicts infiltrative growth of polymorphous tumour cells with discontinuity of upper CAM epithelium. The tumour cells and cell fragments are in loose association. In the center is a large area of Matrigel® visible (green arrow). (3A)-(3E) The xenograft grown under the influence of Geltrex™. This tumour shows cells with mitotic figures and prominent nucleoli in compact cellular association. No invasive growth detectable.

Under the influence of Matrigel®, the cell line 92.1 shows a nodular shape with infiltrative growth into the CAM epithelium as well as partly spindle-shaped to multipolar cell bodies and melanocytic pigment inclusions. Matrigel® extends reticularly from the tumour base into the periphery, which also contains some small vessels (fig. 12 2B-E). The medium condition shows a thin rim of polymorphic tumour cells with several prominent nucleoli and immigration of immature chicken erythrocytes (normoblasts) into the basal sections of the cell fringe (see fig. 12 1B-E). In combination with Geltrex™, polymorphic tumour cells with pyknotic nucleoli are visible in the loose cell fringe (see fig. 12 3B-E).

In combination with Matrigel®, the OMM-2.3 cell line shows invasive tumour growth with intact upper CAM epithelium. The round tumour cell bodies show crescent-shaped nuclei as well as occasionally two nuclei per cell, which vary in orientation. The cells are densely clustered, with vessels visible in between (see fig. 13 2B-E). Both the Geltrex™ and the medium condition show a dense narrow fringe of polymorphous tumour cells (see fig. 13 1B-E and 3B-E).

The OMM-1 cell line forms tumours together with Matrigel® and grows invasively into the CAM. Polymorphous cells with pathological nucleus-plasma relation as well as pyknotic nuclei and partly spindle-shaped cell bodies are visible. Residues of Matrigel® can also be observed here (see fig. 14 2B-E). With regard to the medium condition, an intact CAM epithelium and a discontinuous narrow rim of tumour cell fragments can be seen (see fig. 14 1B-E). In comparison to the medium condition, the cells show a polymorphic tumour cell seam in a loose association with isolated mitotic figures when Geltrex™ is considered. The CAM epithelium is not intact (see fig. 14 3B-E)

Large areas of Matrigel® can be observed in the tumour of the Mel270 cell line. There is invasive growth of the tumour into the discontinuous CAM epithelium. The polymorphic tumour cells and cell fragments are in loose association (see fig. 15 2B-E). Under the influence of Geltrex™, a compact cell association developed with tumour cells that show prominent nucleoli and mitotic figures, but do not grow invasively (see fig. 15 3B-E). In the medium condition, the tumour cells appear as a discontinuous narrow fringe of polymorphic tumour cells (see fig. 15 1B-E).

3.2. Melphalan as a Potential Drug

3.2.1. Macroscopic Tumour Formation

The three uveal melanoma cell lines formed different tumours, whereby their macroscopic differences depending on the treatment condition (control vs. treated) will be described below. As in the first experiment, cell line 92.1 formed brown, sometimes irregularly bordered to nodular tumours. Considering the tumours treated with Melphalan, their appearance shows a nodular structure and a much darker brown to black colour, which can be easily observed in direct comparison (see fig. 16-18). The macroscopic tumours of the cell lines OMM-2.3 and Mel270 appeared as irregularly bordered transparent to whitish tumours. No macroscopic differences could be observed between treated and untreated tumours in either cell line (see fig. 19-22)

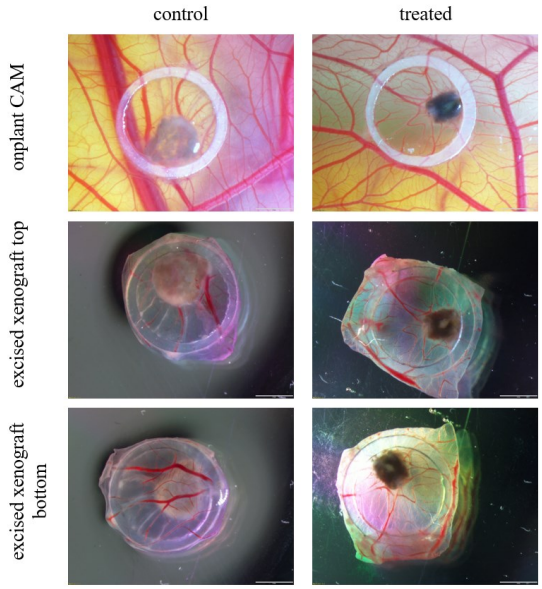

Figure 16. Macroscopic comparison of an untreated and treated CAM tumour of cell line 92.1. The untreated xenograft appears brownish in colour, whereas the treated xenograft appears dark to black-brown. Scale bar: 2mm.

3.2.2. Histological Analysis

The histological results of the second experiment are summarised in the following six figures (fig. 17-22). Two figures are used for each cell line to graphically represent the tumours treated with Melphalan as well as the untreated tumours. For this purpose, the respective onplant on the CAM and the hematoxylin and eosin staining in 40x, 100x and 400x magnification are first used as an overview. In addition, the immunohistochemistry staining with Ki-67 and pancytokeratin (CK), which was performed for one tumour of the respective group, is included.

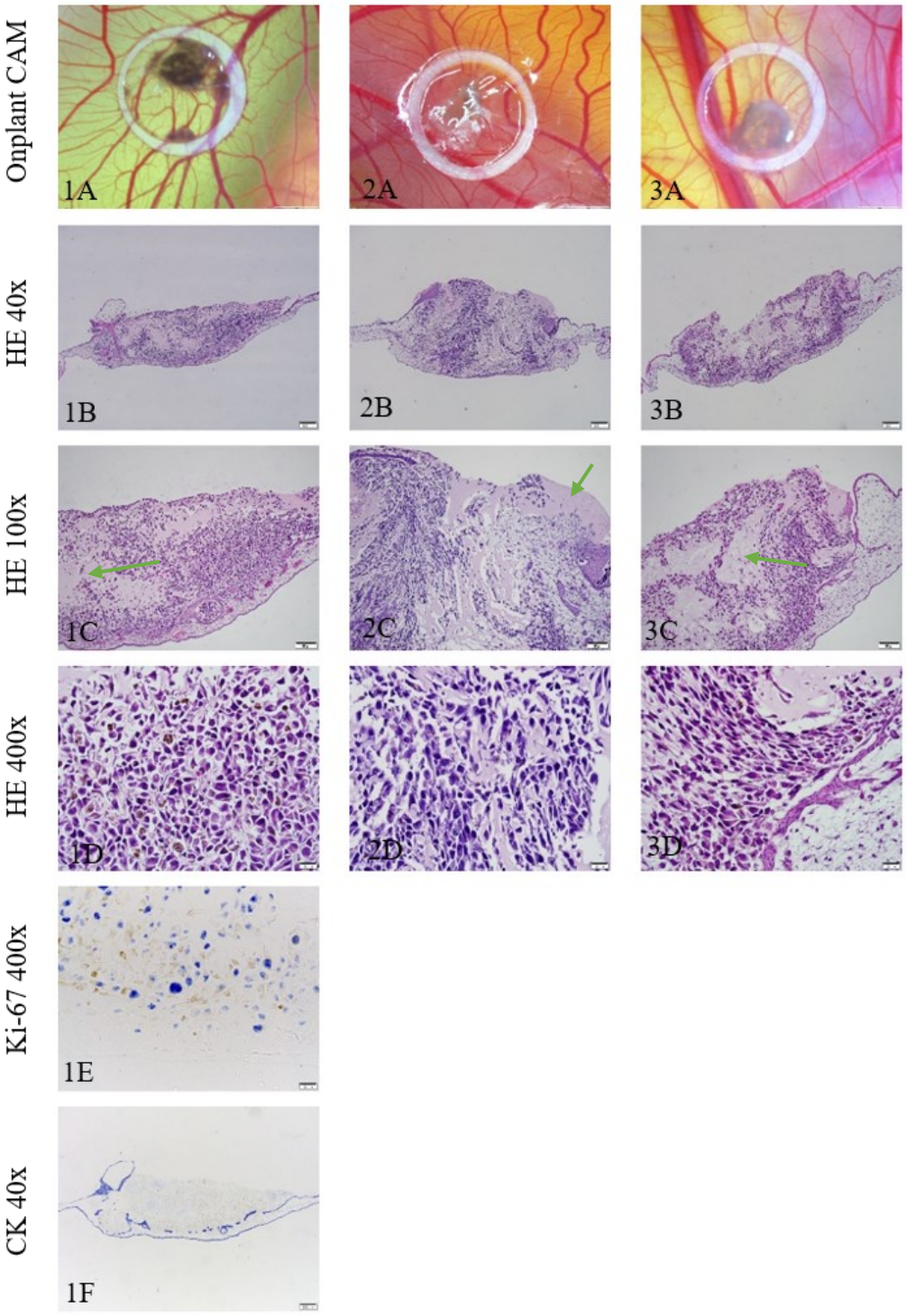

Figure 17. Untreated CAM tumours of the cell line 92.1. Images of the onplant on the CAM labelled (1A)-(3A) serve as an overview for the following HE and immunhistochemical stains, scale bar: 2mm. The HE stains were photographed at 40x, 100x and 400x magnification, scale bar (1B)- (3B): 200µm, (1C)- (3C): 100µm, (1D)- (3D): 20µm. Ki-67 staining was photographed at 400x magnification while CK staining was photographed at 40x magnification. Ki-67 as well as CK positiv cells appear blue. The tumours show infiltrative growth into the CAM epithelium. The polymorphic cells present with melanocytic pigment inclusions as well as multipolar to spindle shaped cell bodies. Extensive inclusions of Matrigel® are present in all tumours (green arrow). There are 32 Ki-67 positive cells at 400x magnification (fig. 1E). CK staining proofs infiltrative growth of the tumour into the CAM epithelium (fig. 1F).

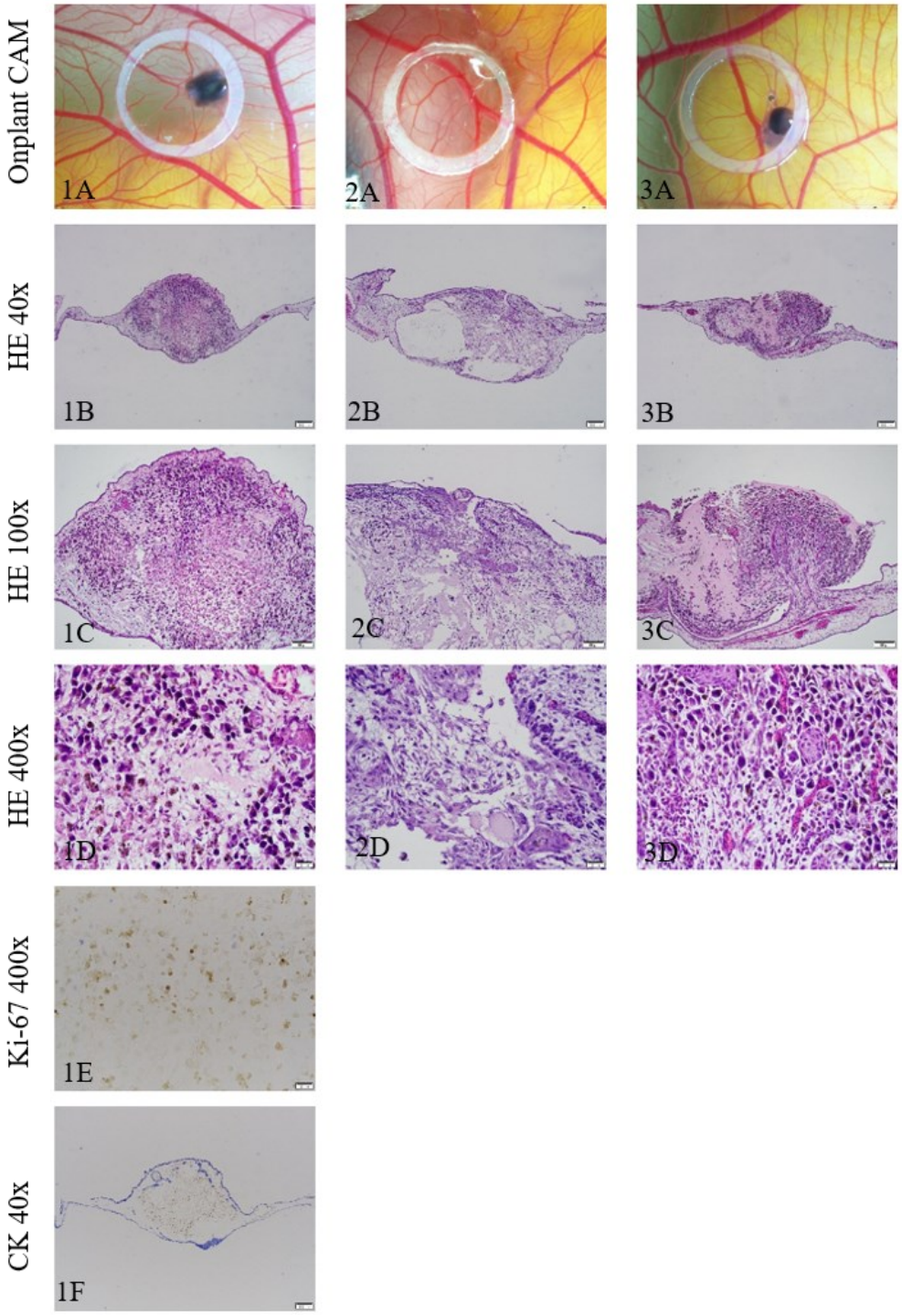

Figure 18. Treated CAM tumours of the cell line 92.1. Images of the onplant on the CAM labelled (1A)-(3A) serve as an overview for the following HE and immunhistochemical stains, scale bar: 2mm. The HE stains were photographed at 40x, 100x and 400x magnification, scale bar (1B)- (3B): 200µm, (1C)- (3C): 100µm, (1D)- (3D): 20µm. Ki-67 staining was photographed at 400x magnification while CK staining was photographed at 40x magnification. Ki-67 as well as CK positiv cells appear blue. Pyknotic nuclei, cell fragments and brown pigments can be observed in the invasively growing tumours. Some of the cells appear multipolar to spindle-shaped. In addition, increased vascularisation can be observed. There are three Ki-67 positive cells at 400x magnification (fig. 1E), scale bar: 20µm. CK staining proofs infiltrative growth of the tumour into the CAM epithelium, scale bar: 200µm (fig. 1F).

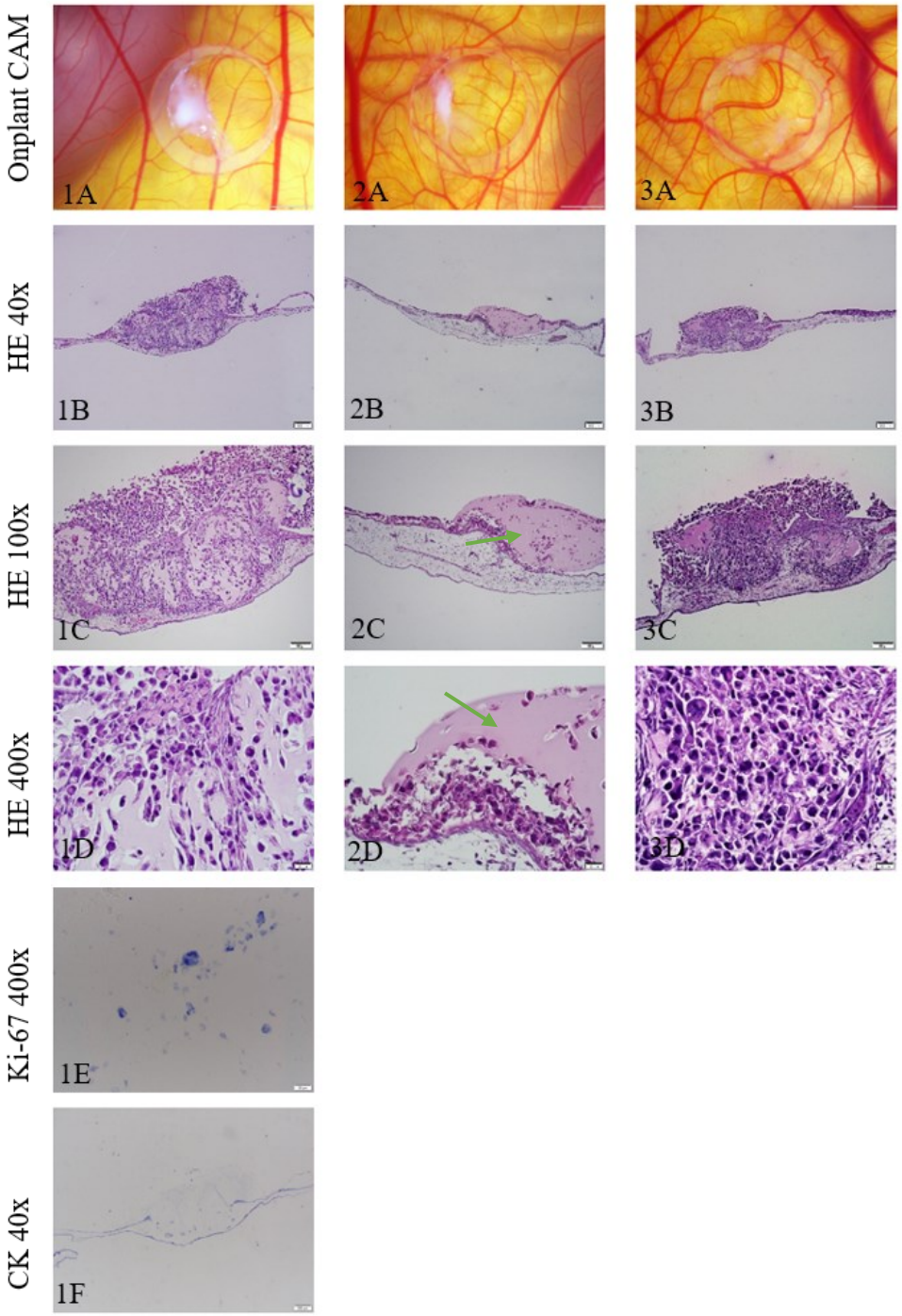

Figure 19. Untreated CAM tumours of the cell line OMM-2.3. Images of the onplant on the CAM labelled (1A)-(3A) serve as an overview for the following HE and immunhistochemical stains, scale bar: 2mm. The HE stains were photographed at 40x, 100x and 400x magnification, scale bar (1B)-(3B): 200µm, (1C)- (3C): 100µm, (1D)- (3D): 20µm. Ki-67 staining was photographed at 40x magnification while CK staining was photographed at 4x magnification. Ki-67 as well as CK positiv cells appear blue. Two out of three tumours grow invasive into the CAM. Their cells are loosely clustered and characterised by a pathological nuclear-cytoplasmic ratio and in some cases round to crescent-shaped nuclei (see fig. 1A-1F, 3A-3D). In the non-infiltrative tumour, Matrigel® can be seen as a large area (green arrow) next to pyknotic nuclei and cell fragments (see fig. 2A-2D). There are ten Ki-67 positive cells at 400x magnification, scale bar 20µm (fig. 1E). CK staining proofs infiltrative growth of the tumour into the CAM epithelium, scale bar: 200µm (fig. 1F).

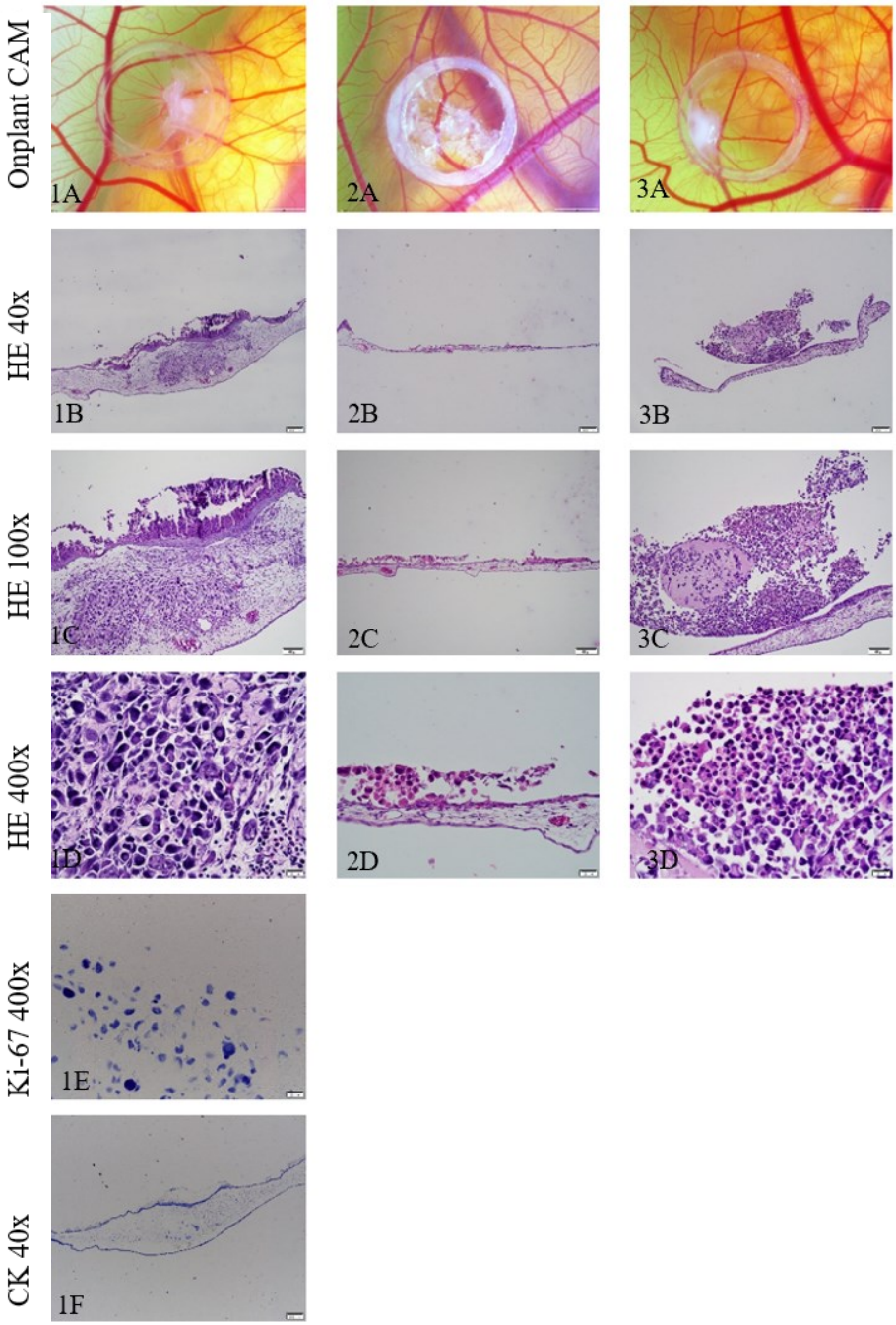

Figure 20. Treated CAM tumours of the cell line OMM-2.3. Images of the onplant on the CAM labelled (1A)-(3A) serve as an overview for the following HE and immunhistochemical stains, scale bar: 2mm. The HE stains were photographed at 40x, 100x and 400x magnification, scale bar (1B)-(3B): 200µm, (1C)- (3C): 100µm, (1D)- (3D): 20µm. Ki-67 staining was photographed at 400x magnification while CK staining was photographed at 40x magnification. Ki-67 as well as CK positiv cells appear blue. Two of the three tumours did not grow invasive into the CAM epithelium. In both xenografts, the small tumour cells sit loosely on the upper epithelium of the CAM and have a roundish nucleus (see fig 2A-2D, 3A-3D). One of the two tumours shows just a seam of the described cells with cell fragments (see fix. 2A-2D). The cells that have grown infiltratively into the CAM show a pathological nuclear-cytoplasmic ratio and a polymorphic tumour cell pattern with sometimes two nuclei per cell while the top of the upper CAM epithelium shows necrotic tumor cells (see fig. 1A-1F). There are 18 Ki-67 positive cells at 400x magnification, scale bar: 20µm (fig. 1E). CK staining proofs infiltrative growth of the tumour into the CAM, scale bar: 200µm (fig. 1F).

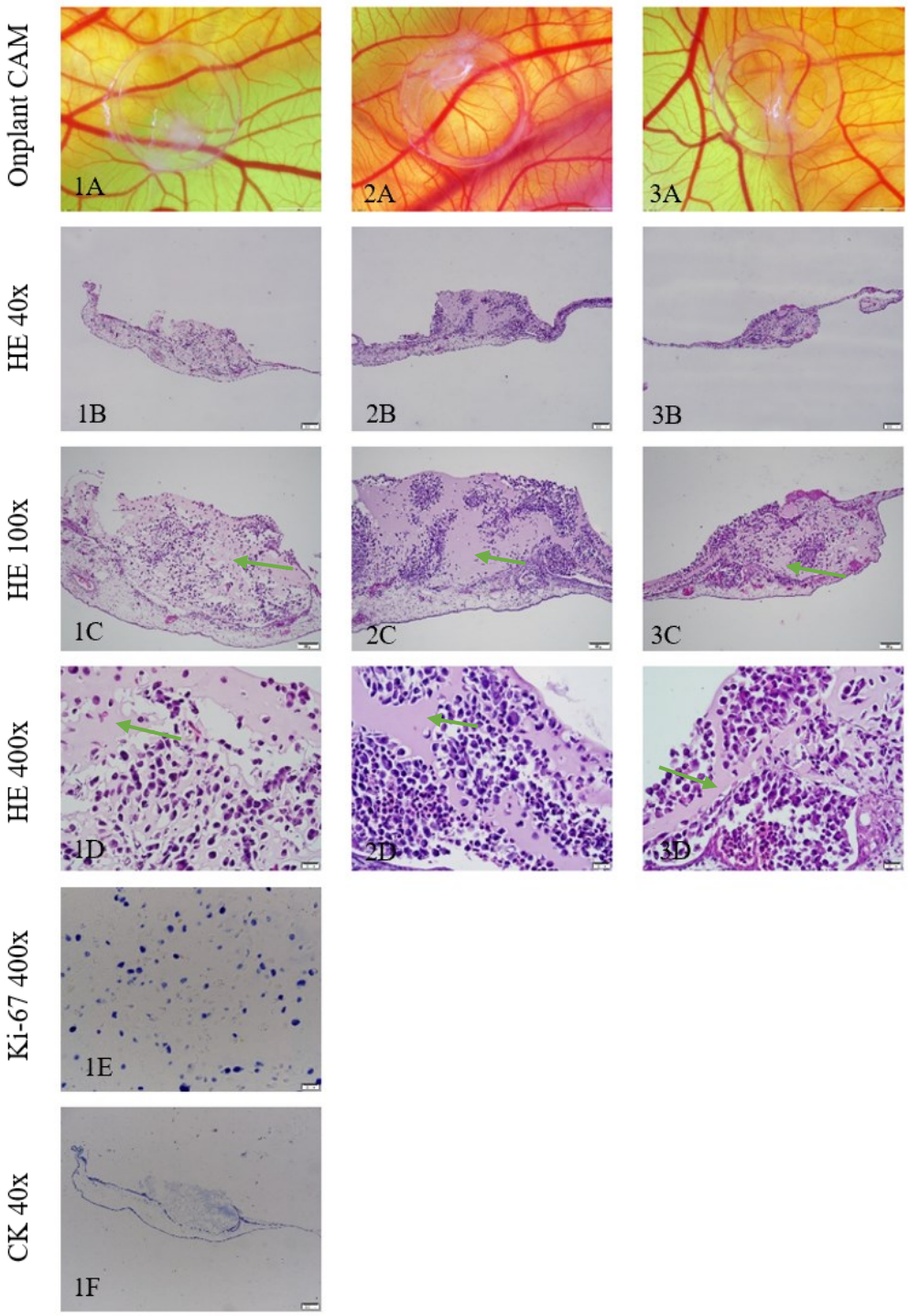

Figure 21. Untreated CAM tumours of the cell line Mel270. Images of the onplant on the CAM labelled (1A)-(3A) serve as an overview for the following HE and immunhistochemical stains, scale bar: 2mm. The HE stains were photographed at 40x, 100x and 400x magnification, scale bar (1B)-(3B): 200µm, (1C)- (3C): 100µm, (1D)- (3D): 20µm. Ki-67 staining was photographed at 400x magnification while CK staining was photographed at 40x magnification. Ki-67 as well as CK positiv cells appear blue. The tumours grow invasive into the CAM epithelium with predominantly small tumour cells. The cells are loosely clustered and show marginal nucelus and a pathological nucleus-cytoplasm ratio. Areas of Matrigel® between the tumour cells can also be observed (green arrow). There are 31 Ki-67 positive cells at 400x magnification, scale bar: 20µm (fig. 1E). CK staining proofs infiltrative growth of the tumour into the CAM epithelium, scale bar: 200µm (fig. 1F).

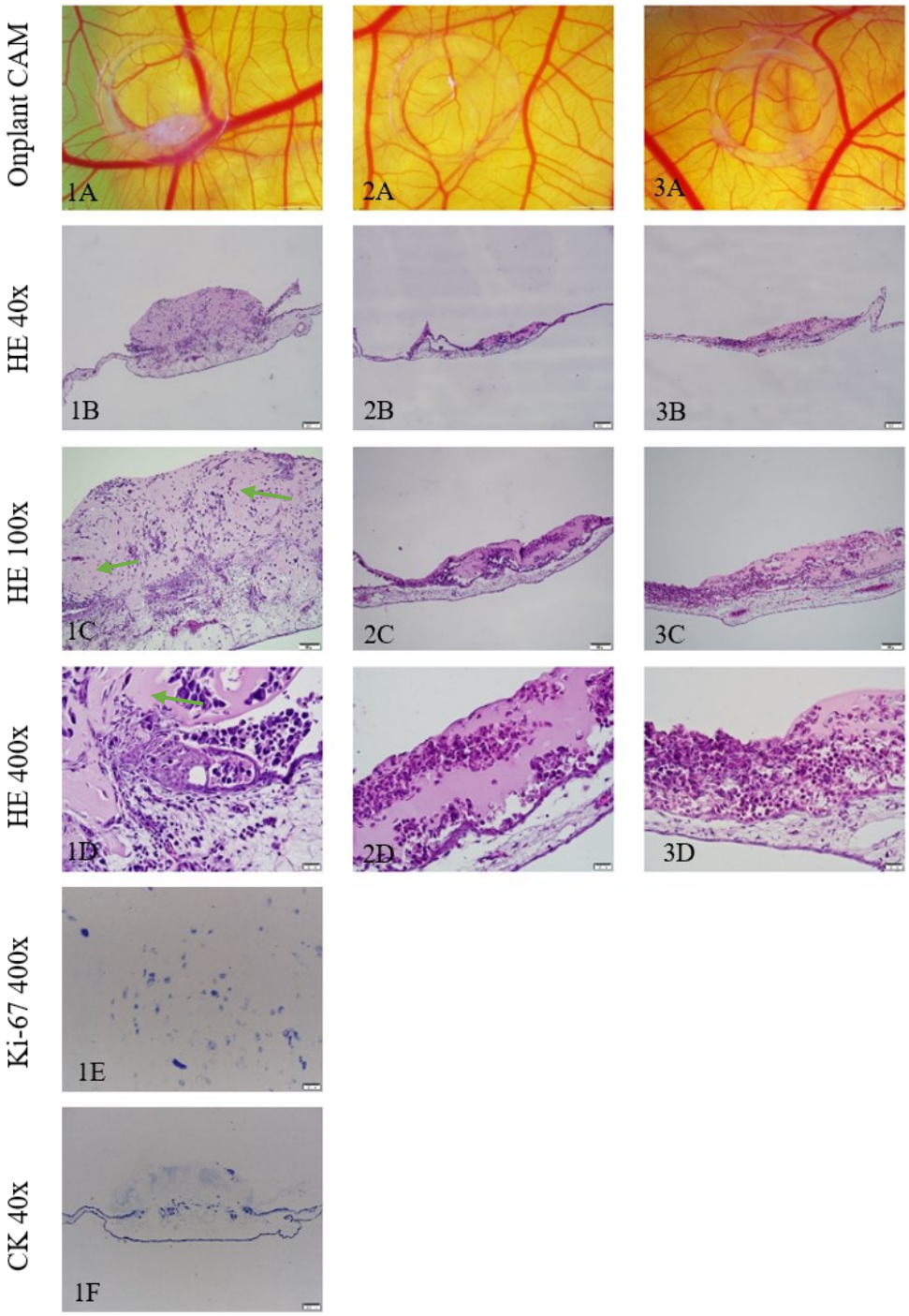

Figure 22. Treated CAM tumours of the cell line Mel270. Images of the onplant on the CAM labelled (1A)-(3A) serve as an overview for the following HE and immunhistochemical stains, scale bar: 2mm. The HE stains were photographed at 40x, 100x and 400x magnification, scale bar (1B)- (3B): 200µm, (1C)- (3C): 100µm, (1D)- (3D): 20µm. Ki-67 staining was photographed at 400x magnification while CK staining was photographed at 40x magnification. Ki-67 as well as CK positiv cells appear blue. Two of the three tumours treated with Melphalan show no infiltrative growth, their dense tumour cell mass shows blurred cell borders as well as pyknotic nuclei and cell fragments (see fig. 2A-2D, 3A-3D). The infiltratively growing tumour is permeated by Matrigel® (green arrow), polymorphic tumour cells with pathological nuclear-plasma ratios and isolated vessels are visible (see fig. 1A-1F). There are 17 Ki-67 positive cells at 400x magnification, scale bar: 20µm (fig. 1E). CK staining proofs infiltrative growth of the tumour into the CAM epithelium, scale bar: 200µm (fig. 1F).

The untreated tumours of cell line 92.1 show infiltrative growth into the CAM epithelium. The cells themselves appear polymorphic with melanocytic pigment inclusions and predominantly mulitpolar to spindle shaped cell bodies. Matrigel® appears as a flat inclusion in the tumour tissue (see fig. 17). The treated tumour cells show infiltrative growth with predominantly pyknotic nuclei and cell fragments as well as melanocytic pigment. In some areas, cells with multipolar to spindle-shaped cell bodies can be seen between the vessels (see fig. 18). If one compares the treated and untreated tumours with regard to their Ki-67 activity, the untreated tumours show 32 Ki-67 positive cells and the treated tumours three positive cells.

The untreated tumour cells OMM-2.3 grow infiltratively into the CAM epithelium in two out of three tumours. The cells are loosely clustered and are characterised by a pathological nuclear-cytoplasmic ratio and in some cases round to crescent-shaped nuclei (see fig. 19 1A-1F, 3A-3D). In the non-infiltrative tumour, Matrigel® can be seen as a large area next to pyknotic nuclei and cell fragments (see fig. 19 2A-D). In contrast, the treated cells show a microscopically different picture compared to each other. Two of the three tumours did not grow infiltratively into the CAM epithelium. In both xenografts, the small tumour cells sit loosely on the upper epithelium of the CAM and have a roundish nucleus (see fig. 20 2A-2D, 3A-3D). In one of the two tumours, the cells did not grow well on the CAM, showing a seam of the described cells with cell fragments (see fig 20 2A-2D). The cells that have grown infiltratively into the CAM show a pathological nuclear-cytoplasmic ratio and a polymorphic tumour cell pattern with sometimes two nuclei per cell while the top of the upper CAM epithelium shows necrotic tumor cells (see fig. 20 1A-F). Regarding the Ki-67 activity the untreated tumours count ten while the treated tumours count 18 positive cells.

The untreated cells of the Mel270 cell line can be characterised by infiltrative growth of the predominantly small tumour cells. The cells are loosely clustered and show a marginal nucleus and a pathological nucleus-cytoplasm ratio. Areas of Matrigel® can also be observed (see fig. 21). Two of the three tumours treated with Melphalan show no infiltrative growth, their dense tumour cell mass shows blurred cell borders as well as pyknotic nuclei and cell fragments (see fig. 22 2A-2D, 3A-3D). The infiltratively growing tumour is permeated by Matrigel®, polymorphic tumour cells with pathological nuclear-plasma ratios and isolated vessels are visible (see fig. 22 1A-1F). The untreated tumours show a Ki-67 activity of 31 while the treated tumors show an activity of 17.
In all three cell lines, the CAM of the treated tumours was unaffected by Melphalan.

4. Discussion

In the first sub-experiment, this study focussed on which matrix condition provides the most optimal growth conditions for the cultured uveal melanoma cell lines for the ex ovo CAM assay. In addition to cell culture medium, Matrigel® and Geltrex™ were available as matrices. The results of this study show that the respective investigated cell lines 92.1, OMM-2.3, OMM-1 and Mel270 form the macroscopically largest tumours under the influence of Matrigel®. The tumours grew firmly on the CAM and showed increased vascularisation. Hematoxylin eosin staining enabled the individual structures in the histological section to be clearly differentiated from each other, the nuclei turned blue and the cytoplasm turned pink, allowing a descriptive approach to the assessment of the tumours and the cell image. Microscopically, the tumours showed invasive growth in the CAM epithelium compared to the other matrix conditions, as well as increased vascularisation and a proliferating cell image. Similar results were described in a study by Sokolenko et al. (2022:5-6). This study dealt with the optimisation of the in ovo CAM assay for the examination of uveal melanoma tumour spheroids. Here, Matrigel® was also shown to be the most successful matrix under which the spheroids proliferate and grow adhesive on the CAM. Good tumour growth on the CAM was also shown in cutaneous melanoma under the influence of Matrigel® (Rinner et al., 2017:3-10). According to a systematic review study by Mesas et al. (2024:17), in which over 74 studies were analysed, it was shown that Matrigel® is most frequently used as a matrix to stimulate tumour growth, regardless of whether the CAM assay uses the in ovo or ex ovo technique. In this study it was shown that Matrigel® is the most successful matrix for the ex ovo CAM assay compared to cell culture medium RPMI-1640 and Geltrex™ for the growth of uveal melanoma cell lines.

In comparison, the Mel270 cell line formed the macroscopically smallest tumours. This result was surprising as the cell line in cell culture showed a similar growth and splitting rate as the other cells. At the time of the first experiment, a cell viability of 86.1% was achieved and at the time of the second experiment a viability of 95.1%, which ultimately provides good conditions for growth on the CAM. This cell line in particular would possibly benefit from a larger number of cells per onplant, so that more cells would be available that could ultimately form larger tumours.

In the context of the second experiment, it is important to mention that it is intended to be a pilot experiment that serves as a basis for further experiments. The second experiment focussed on the effect of the potential drug Melphalan on the respective uveal melanoma

cell lines. The dosage of Melphalan was derived from the study by Munier et al. (2019:2-56). The aim was to select a dosage that showed an effect on the onplant without prematurely terminating the experiment due to the possible toxic effect on the chicken embryo. 10µl Melphalan was applied with a concentration of 10µl/ml per onplant. After ten minutes, the agent was washed five times with 10µl cell culture medium RPMI-1640 and a pipette to remove it from the onplant. Overall, the dosage proved to be adequate, as none of the chicken embryos dropped out of the experiment prematurely after application of Melphalan. In contrast to the Mel270 and OMM-2.3 cell lines, there was a macroscopic difference between the treated and non-treated tumours in cell line 92.1. The treated tumours stood out due to their dark brown to black-brown colour, whereas the untreated tumours appeared brownish. The black-brown colour of the treated tumours can be interpreted as possible necrosis and shows that Melphalan has an effect on this cell line. This interpretation was confirmed in the histological section, as an increased number of pyknotic nuclei, cell fragments and free pigment was observed in the treated tumours with a considerable reduction in Ki-67 activity. The reason for this could be the affinity of Melphalan to pigmented melanoma cells already described in section 1.2.3.2. Pigmented melanoma cells exhibit an increased consumption of the amino acids phenylalanine and tyrosine, as they require these for the production of melanosomes. Melphalan or L-phenylalanine mustard could possibly be increasingly taken up by melanocytes due to its structural similarity to phenylalanine and thus have an increased effect as an alkylant in these cells (Bergel & Stock, 1953, cited in Samuels & Bitran, 1995:1786, Benathan et al., 1992:311-312). A macroscopic difference between the treated and non-treated tumours of the non-pigmented cell lines OMM-2.3 and Mel270 could not be observed. A possible reason for the absence of pigmentation in these cell lines, which were both derived from the same organism, could be that the primary tumour from which the Mel270 cell line was cultivated was irradiated prior to enucleation. This means that the primary tumour and its metastases, from which the OMM-2.3 cell line was ultimately cultivated, could have lost their pigmentation due to irradiation. The histological section shows an inconclusive cell image for both cell lines. Two out of three of the untreated tumours of the OMM-2.3 cell line show infiltrative growth, which is a sign of proliferation. The treated OMM-2.3 tumours show infiltrative growth in one of three tumours. In the histological section of this tumour, in addition to necrotic tumour cells on the upper CAM epithelium, proliferating cells can be observed within the CAM, which may have been able to secure a survival advantage over Melphalan through infiltrative growth. The results of the Ki-67 staining also support this interpretation, because the only proliferating tumour cells

are located within the CAM. It is possible that Melphalan did not penetrate these cells, in contrast to the tumour cells on the upper CAM epithelium. This could be related to the method of application, as Melphalan was applied locally to the tumour cells using a pipette. It is possible that an intra-arterial application of Melphalan into the vascular system would have a different effect and reach infiltratively growing cells in higher concentrations. There are already studies that have investigated the intra-arterial application of fluorescin into the CAM using 33-gauge needles (Leng et al., 2004:431-432). It is possible that the intra-arterial application of Melphalan in this setting could also provide further information on the effect of Melphalan on the OMM-2.3 cell line. All tumours of the Mel270 cell line grow infiltratively into the CAM epithelium and thus show proliferation. Two of the treated tumours of this cell line show no infiltrative growth but predominantly necrotic tumour mass. The infiltratively growing tumour shows large areas of Matrigel® in addition to the predominantly vital tumour cells. These large Matrigel® inclusions may indicate that the tumour cells were unable to consume Matrigel®. The Ki-67 activity in the cells of this cell line is lower in the treated tumours than in the untreated tumours, which may indicate a possible effect of Melphalan. It is important to note that the Ki-67 staining is not optimised for analysis due to the low background signal. It is therefore necessary to establish a working immunohistochemistry staining protocol with Ki-67 to ultimately analyse differences in proliferation between all treated and non-treated tumours.

At this point, it is important to highlight that the CAM model as a whole provides a very goood model for researching tumours and the effects of potential drugs on them due to its immunodeficiency and its rapidly reproducible and cost-effective method. However, it is also important to mention limitations of the method. For example, the short post-treatment observation period limits the significance of the long-term effect of potential therapeutic agents and therefore only an initial response to the therapy can be investigated. In addition, the administration of drugs is partly limited by the solubility of the molecules, so the drugs must be solubilised befor they can be injected. Furthermore, drugs cannot be administered orally (Fischer et al., 2022:17-18).

Finally, the application of Melphalan may have influenced the results. Melphalan was applied to one onplant per CAM, so that systemic effects influencing the results of untreated onplants cannot be ruled out. It is therefore possible that Melphalan was absorbed via the vascular system during the ten-minute dwell time on the onplant and thus had an effect on the other onplants of the CAM, thereby biasing the results.

Overall, the tumours grew well on the CAM and the CAM proved to be a suitable model for investigating the research questions. The dosage of Melphalan is considered adequate. A clear effect of the drug in the experiment could only be determined for cell line 92.1. The method of application should be adapted for future experiments in order to control systemic effects of Melphalan on the other onplants. It is also necessary to establish a working immunhistochemistry staining protocol for Ki-67 staining in order to evaluate differences between treated and untreated tumours. Further research is needed to ultimately assess the value of Melphalan and its potential effect on uveal melanoma.

References

Abdel-Rahman, M. H., Pilarski, R., Cebulla, C. M., Massengill, J. B., Christopher, B. N., Boru, G., … Davidorf, F. H. (2011) 'Germline BAP1 mutation predisposes to uveal melanoma, lung adenocarcinoma, meningioma, and other cancers.' *Journal of Medical Genetics, 48(12), 856–859.* doi:10.1136/jmedgenet-2011-100156

Alfaar, A. S., Saad, A., Wiedemann, P., & Rehak, M. (2022) ´The epidemiology of uveal melanoma in Germany: a nationwide report of incidence and survival between 2009 and 2015´. *Graefe's Archive for Clinical and Experimental Ophthalmology*, 260(5), 1723–1731. https://doi.org/10.1007/s00417-021-05317-7

Amaro, A., Gangemi, R., Piaggio, F., Angelini, G., Barisione, G., Ferrini, S., & Pfeffer, U. (2017)'The biology of uveal melanoma.' *Cancer and Metastasis Reviews, 36(1), 109–140.* doi:10.1007/s10555-017-9663-3

Amirouchene-Angelozzi, N., Nemati, F., Gentien, D., Nicolas, A., Dumont, A., Carita, G., (…), Roman-Roman, S. (2014)´ Establishment of novel cell lines recapitulating the genetic landscape of uveal melanoma and preclinical validation of mTOR as a therapeutic target´. *Molecular oncology*, *8*(8), 1508–1520. https://doi.org/10.1016/j.molonc.2014.06.004

Bauer, J., Büttner, P., Wiecker, T. S., Luther, H., & Garbe, C. (2005) 'Risk factors of incident melanocytic nevi: a longitudinal study in a cohort of 1,232 young German children'. *International journal of cancer*, *115*(1), 121–126. https://doi.org/10.1002/ijc.20812

Bechrakis, N. E., Bornfeld, N., Heindl, L. M., Skoetz, N., Leyvraz, S., & Joussen, A. M. (2021) 'Uveal Melanoma - Standardised Procedure in Diagnosis, Therapy and Surveillance. Das uveale Melanom – standardisiertes Vorgehen in Diagnostik, Therapie und Nachsorge.' *Klinische Monatsblätter für Augenheilkunde*, *238*(7), 761–772. https://doi.org/10.1055/a-1534-0198

Benathan, M., Alvero-Jackson, H., Mooy, A.-M., Scaletta, C., & Frenk, E. (1992) 'Relationship between melanogenesis, glutathione levels and melphalan toxicity in human melanoma cells.' *Melanoma Research, 2(5), 305–314.* doi:10.1097/00008390-199212000-00003

Breitbart, M., Garbe, C., Büttner, P., Weiss, J., Soyer, H., Stocker, (…), & Orfanos, C. (1997) 'A case-control study of the German Central Malignant Melanoma Registry.' *Acta Dermato-Venereologica*, 77(5), pp. 374–378. doi: 10.2340/0001555577374378.

Bultynck, G., & Campanella, M. (2017) 'Tumor suppressive Ca^{2+} signaling is driven by IP_3 receptor fitness.' *Cell stress*, *1*(2), 73–78. https://doi.org/10.15698/cst2017.11.109

Chang, A. E., Karnell, L. H., & Menck, H. R. (1998) 'The National Cancer Data Base report on cutaneous and noncutaneous melanoma: a summary of 84,836 cases from the past decade. The American College of Surgeons Commission on Cancer and the American Cancer Society.' *Cancer*, *83*(8), 1664–1678. https://doi.org/10.1002/(sici)1097-0142(19981015)83:8<1664::aid-cncr23>3.0.co;2-g

Chattopadhyay, C., Kim, D. W., Gombos, D. S., Oba, J., Qin, Y., Williams, M. D., … & Patel, S. P. (2016) 'Uveal melanoma: From diagnosis to treatment and the science in between.' *Cancer, 122(15), 2299–2312.* doi:10.1002/cncr.29727

Chen, P. W., Murray, T. G., Uno, T., Salgaller, M. L., Reddy, R., & Ksander, B. R. (1997) ´Expression of MAGE genes in ocular melanoma during progression from primary to metastatic disease´. *Clinical & experimental metastasis*, *15*(5), 509–518. https://doi.org/10.1023/a:1018479011340

Davis, E.J., Johnson, D.B., Sosman, J.A., & Chandra, S. (2018) 'Melanoma: What do all the mutations mean?' *Cancer*, 124: 3490-3499. https://doi.org/10.1002/cncr.31345

Decatur, C. L., Ong, E., Garg, N., Anbunathan, H., Bowcock, A. M., Field, M. G., & Harbour, J. W. (2016) 'Driver Mutations in Uveal Melanoma: Associations With Gene Expression Profile and Patient Outcomes.' *JAMA ophthalmology*, *134*(7), 728–733. https://doi.org/10.1001/jamaophthalmol.2016.0903

Demirkan, S., Onaran, Z., Samav, G., Özkal, F., Yumuşak, E., Gündüz, Ö., & Karabulut, A. (2018) 'Decreased choroidal thickness in vitiligo patients.' *BMC ophthalmology*, *18*(1), 126. https://doi.org/10.1186/s12886-018-0796-0

De Waard-Siebinga, I., Blom, D. J., Griffioen, M., Schrier, P. I., Hoogendoorn, E., Beverstock, G., (…), Jager, M. J. (1995)´ Establishment and characterization of an

uveal-melanoma cell line′. *International journal of cancer*, *62*(2), 155–161. https://doi.org/10.1002/ijc.2910620208

Diener-West, M., Reynolds, S. M., Agugliaro, D. J., Caldwell, R., Cumming, K., Earle, J. D.,..., & Collaborative Ocular Melanoma Study Group (2005). Development of metastatic disease after enrollment in the COMS trials for treatment of choroidal melanoma: Collaborative Ocular Melanoma Study Group Report No. 26. *Archives of ophthalmology (Chicago, Ill. : 1960)*, *123*(12), 1639–1643. https://doi.org/10.1001/archopht.123.12.1639

Ewens, K. G., Kanetsky, P. A., Richards-Yutz, J., Purrazzella, J., Shields, C. L., Ganguly, T., & Ganguly, A. (2014) 'Chromosome 3 status combined with BAP1 and EIF1AX mutation profiles are associated with metastasis in uveal melanoma.' *Investigative ophthalmology & visual science*, *55*(8), 5160–5167. https://doi.org/10.1167/iovs.14-14550

Ewens, K. G., Lalonde, E., Richards-Yutz, J., Shields, C. L., & Ganguly, A. (2018) 'Comparison of Germline versus Somatic BAP1 Mutations for Risk of Metastasis in Uveal Melanoma.' *BMC cancer*, *18*(1), 1172. https://doi.org/10.1186/s12885-018-5079-x

Fergelot, P., Bernhard, J. C., Soulet, F., Kilarski, W. W., Leon, C., Courtois, N., ..., & Bikfalvi, A. (2013) 'The experimental renal cell carcinoma model in the chick embryo.' *Angiogenesis* 16, 181–194. https://doi.org/10.1007/s10456-012-9311-z

Fischer, D., Fluegen, G., Garcia, P., Ghaffari-Tabrizi-Wizsy, N., Gribaldo, L., Huang, R. Y., …, & Schneider-Stock, R. (2022) 'The CAM Model-Q&A with Experts.' *Cancers*, 15(1), 191. https://doi.org/10.3390/cancers15010191

Ghaffari-Tabrizi-Wizsy, N., Passegger, C. A., Nebel, L., Krismer, F., Herzer-Schneidhofer, G., Schwach, G., & Pfragner, R. (2019) 'The avian chorioallantoic membrane as an alternative tool to study medullary thyroid cancer.' *Endocrine connections*, *8*(5), 462–467. https://doi.org/10.1530/EC-18-0431

Gobin, Y. P. (2011) 'Intra-arterial Chemotherapy for the Management of Retinoblastoma.' *Archives of Ophthalmology, 129(6), 732.* doi:10.1001/archophthalmol.2011.5

Griewank, K. G., Yu, X., Khalili, J., Sozen, M. M., Stempke-Hale, K., Bernatchez, C., (…), Woodman, S. E. (2012) ′Genetic and molecular characterization of uveal

melanoma cell lines′. *Pigment cell & melanoma research*, *25*(2), 182–187. https://doi.org/10.1111/j.1755-148X.2012.00971.x

Han, A., Purwin, T. J., & Aplin, A. E. (2021) 'Roles of the BAP1 Tumor Suppressor in Cell Metabolism.' *Cancer research*, *81*(11), 2807–2814. https://doi.org/10.1158/0008-5472.CAN-20-3430

Hughes, C. S., Postovit, L. M., & Lajoie, G. A. (2010) 'Matrigel: A complex protein mixture required for optimal growth of cell culture.' *PROTEOMICS, 10(9), 1886–1890.* doi:10.1002/pmic.200900758

Jager, M. J., Magner, J. A., Ksander, B. R., & Dubovy, S. R. (2016) ′Uveal Melanoma Cell Lines: Where do they come from?′ (An American Ophthalmological Society Thesis). *Transactions of the American Ophthalmological Society*, *114*, T5.

Jampol, L. M., Moy, C. S., Murray, T. G., Reynolds, S. M., Albert, D. M., Schachat,…, & COMS Follow-up of Plaqued Eyes Working Group (2020) 'The COMS Randomized Trial of Iodine 125 Brachytherapy for Choroidal Melanoma: IV. Local Treatment Failure and Enucleation in the First 5 Years after Brachytherapy. COMS Report No. 19.' *Ophthalmology*, *127*(4S), S148–S157. https://doi.org/10.1016/j.ophtha.2020.01.032

Janković, B. D., Isaković, K., Lukić, M. L., Vujanović, N. L., Petrović, S., & Marković, B. M. (1975) 'Immunological capacity of the chicken embryo. I. Relationship between the maturation of lymphoid tissues and the occurrence of cell-mediated immunity in the developing chicken embryo.' *Immunology*, *29*(3), 497–508.

Jensen, D. E., Proctor, M., Marquis, S. T., Gardner, H. P., Ha, S. I., Chodosh, L. A., …, & Rauscher, F. J., (1998) 'BAP1: a novel ubiquitin hydrolase which binds to the BRCA1 RING finger and enhances BRCA1-mediated cell growth suppression.' *Oncogene*, *16*(9), 1097–1112. https://doi.org/10.1038/sj.onc.1201861

Johansson, P., Aoude, L. G., Wadt, K., Glasson, W. J., Warrier, S. K., Hewitt, A. W., …, & Hayward, N. K. (2016) 'Deep sequencing of uveal melanoma identifies a recurrent mutation in PLCB4.' *Oncotarget*, *7*(4), 4624–4631. https://doi.org/10.18632/oncotarget.6614

Koopmans, A. E., Verdijk, R. M., Brouwer, R. W. W., van den Bosch, T. P. P., van den Berg, M. M. P., Vaarwater, J., …, & de Klein, A. (2014) ‚Clinical significance of

immunohistochemistry for detection of BAP1 mutations in uveal melanoma.' *Modern Pathology, 27(10), 1321–1330.* doi:10.1038/modpathol.2014.43

Lamas, N. J., Martel, A., Nahon-Estève, S., Goffinet, S., Macocco, A., Bertolotto, C., …, & Hofman, P. (2021) 'Prognostic Biomarkers in Uveal Melanoma: The Status Quo, Recent Advances and Future Directions.' *Cancers*, *14*(1), 96. https://doi.org/10.3390/cancers14010096

Leng, T., Miller, J. M., Bilbao, K. V., Palanker, D. V., Huie, P., & Blumenkranz, M. S. (2004) 'The chick chorioallantoic membrane as a model tissue for surgical retinal research and simulation.' *Retina (Philadelphia, Pa.)*, *24*(3), 427–434. https://doi.org/10.1097/00006982-200406000-00014

Luyten, G. P., Naus, N. C., Mooy, C. M., Hagemeijer, A., Kan-Mitchell, J., Van Drunen, (…), Luider, T. M. (1996) ´Establishment and characterization of primary and metastatic uveal melanoma cell lines´. *International journal of cancer*, *66*(3), 380–387. https://doi.org/10.1002/(SICI)1097-0215(19960503)66:3<380::AID-IJC19>3.0.CO;2-F

Mallet, J. D., Gendron, S. P., Drigeard Desgarnier, M.-C., & Rochette, P. J. (2013) 'Implication of ultraviolet light in the etiology of uveal melanoma: A review.' *Photochemistry and Photobiology, 90(1), 15–21.* doi:10.1111/php.12161

Martin, M., Maßhöfer, L., Temming, P., Rahmann, S., Metz, C., Bornfeld, …, & Zeschnigk, M. (2013) 'Exome sequencing identifies recurrent somatic mutations in EIF1AX and SF3B1 in uveal melanoma with disomy 3.' *Nature genetics*, *45*(8), 933–936. https://doi.org/10.1038/ng.2674

Moore, A. R., Ceraudo, E., Sher, J. J., Guan, Y., Shoushtari, A. N., Chang, M. T., …, & Chen, Y. (2016) 'Recurrent activating mutations of G-protein-coupled receptor CYSLTR2 in uveal melanoma.' *Nature Genetics*, 48(6), 675–680. doi:10.1038/ng.3549

Munier, F. L., Gaillard, M.-C., Balmer, A., Soliman, S., Podilsky, G., Moulin, A. P., & Beck-Popovic, M. (2012) 'Intravitreal chemotherapy for vitreous disease in retinoblastoma revisited: from prohibition to conditional indications.' *British Journal of Ophthalmology, 96(8), 1078–1083.* doi:10.1136/bjophthalmol-2011-301450

Munier, F. L., Beck-Popovic, M., Chantada, G. L., Cobrinik, D., Kivelä, T. T., Lohmann, D., ..., & Stathopoulos, C. (2019) 'Conservative management of retinoblastoma: Challenging orthodoxy without compromising the state of metastatic grace. "Alive, with good vision and no comorbidity".' *Progress in retinal and eye research*, *73*, 100764. https://doi.org/10.1016/j.preteyeres.2019.05.005

National Library of Medicine (2024) *SF3B1 splicing factor 3b subunit 1*. Available at: https://www.ncbi.nlm.nih.gov/gene/23451 [Accessed: 20.01.2024]

National Library of Medicine (2023) *EIF1AX eukaryotic translation initiation factor 1A X-linked*. Available at : https://www.ncbi.nlm.nih.gov/gene/1964 [Accessed: 19.01.2024]

Olofsson Bagge, R., Nelson, A., Shafazand, A., All-Eriksson, C., Cahlin, C., Elander, N.,…, & Lindnér, P. (2023) 'Isolated Hepatic Perfusion With Melphalan for Patients With Isolated Uveal Melanoma Liver Metastases: A Multicenter, Randomized, Open-Label, Phase III Trial (the SCANDIUM Trial).' *Journal of clinical oncology : official journal of the American Society of Clinical Oncology*, *41*(16), 3042–3050. https://doi.org/10.1200/JCO.22.01705

Rauchegger, T., Blatsios, G., Haas, G. , Zehetner, C., & Bechrakis N. E. (2020) 'Zehn Jahre multimodale Therapie uvealer Melanome an der Universitätsaugenklinik Innsbruck.' *Spektrum Augenheilkunde.* 34, 18–25 . https://doi.org/10.1007/s00717-019-0422-4

Ribatti D. (2017) 'The chick embryo chorioallantoic membrane (CAM) assay.' *Reproductive toxicology (Elmsford, N.Y.)*, *70*, 97–101. https://doi.org/10.1016/j.reprotox.2016.11.004

Ribatti, D., 2014. The chick embryo chorioallantoic membrane as a model for tumor biology. Exp. Cell Res. 328, 314–324. http://dx.doi.org/10.1016/j.yexcr.2014.06.010

Ribatti, D. (2016) 'The chick embryo chorioallantoic membrane (CAM). A multifaceted experimental model*.' Mechanisms of Development, 141, 70–77.* doi:10.1016/j.mod.2016.05.003

Rinner, B., Gandolfi, G., Meditz, K., Frisch, M. T., Wagner, K., Ciarrocchi, A., …, & Zalaudek, I. (2017) 'MUG-Mel2, a novel highly pigmented and well characterized

NRAS mutated human melanoma cell line.' *Scientific reports*, 7(1), 2098. https://doi.org/10.1038/s41598-017-02197-y

Salmon, J. F. (2019) *Kanski's Clinical Ophthalmology: A Systematic Approach*. Amsterdam: Elsevier Health Sciences.

Samuels, B. L., & Bitran, J. D. (1995) 'High-dose intravenous melphalan: a review.' *Journal of Clinical Oncology, 13(7), 1786–1799.* doi:10.1200/jco.1995.13.7.1786

Schallreuter, K. U., Kothari, S., Chavan, B., & Spencer, J. D. (2008) 'Regulation of melanogenesis - controversies and new concepts.' *Experimental dermatology*, *17*(5), 395–404. https://doi.org/10.1111/j.1600-0625.2007.00675.x

Schatz, O., Zalaudek, I., Ghaffari Tabrizi-Wizsy, N., Grechenig, C., Grinninger, P., Haas, A., … & Schwab, C. (2019). 'Melanocytes, Organogenesis, and Angiogenesis: Evidence for More than a Pigment-Producing Capability of Melanocytes.' *Cells Tissues Organs, 1–3.* doi:10.1159/000495908

Shields, J. A., Demirci, H., Mashayekhi, A., Eagle, R. C., Jr, & Shields, C. L. (2019) 'Melanocytoma of the optic disk: A review.' *Indian journal of ophthalmology*, *67*(12), 1949–1958. https://doi.org/10.4103/ijo.IJO_2039_19

Shields, C. L., Douglass, A. M., Beggache, M., Say, E. A. T., & Shields, J. A. (2016). 'Intravitreous chemotherapy for active vitreous seeding from retinoblastoma.' *Retina, 36(6), 1184–1190.* doi:10.1097/iae.0000000000000903

Shields, C. L., Kaliki, S., Rojanaporn, D., Al-Dahmash, S., Bianciotto, C. G., & Shields, J. A. (2012) 'Intravenous and intra-arterial chemotherapy for retinoblastoma.' *Current Opinion in Ophthalmology, 23(3), 202–209.* doi:10.1097/icu.0b013e3283524130

Sokolenko, E. A., Berchner-Pfannschmidt, U., Ting, S. C., Schmid, K. W., Bechrakis, N. E., Seitz, ..., & Fiorentzis, M. (2021) 'Optimisation of the Chicken Chorioallantoic Membrane Assay in Uveal Melanoma Research.' *Pharmaceutics*, *14*(1), 13. https://doi.org/10.3390/pharmaceutics14010013

Sommer, L. (2011) 'Generation of melanocytes from neural crest cells.' *Pigment Cell & Melanoma Research, 24(3), 411–421.* doi:10.1111/j.1755-148x.2011.00834.x

Strojnik, T., Kavalar, R., Barone, T. A., & Plunkett, R. J. (2010) 'Experimental model and immunohistochemical comparison of U87 human glioblastoma cell xenografts on

the chicken chorioallantoic membrane and in rat brains.' *Anticancer research*, *30*(12), 4851–4860.

Sun, X., & Kaufman, P. D. (2018) 'Ki-67: more than a proliferation marker.' *Chromosoma*, *127*(2), 175–186. https://doi.org/10.1007/s00412-018-0659-8

Tschentscher, F., Hüsing, J., Hölter, T., Kruse, E., Dresen, I. G., Jöckel, K. H., …, & Zeschnigk, M. (2003) 'Tumor classification based on gene expression profiling shows that uveal melanomas with and without monosomy 3 represent two distinct entities.' *Cancer research*, *63*(10), 2578–2584.

Tsimpaki, T., Bechrakis, N. E., Seitz, B., Kraemer, M. M., Liu, H., Dalbah, S., …, & Fiorentzis, M. (2023) 'Chick Chorioallantoic Membrane as a Patient-Derived Xenograft Model for Uveal Melanoma: Imaging Modalities for Growth and Vascular Evaluation.' *Cancers*, *15*(5), 1436. https://doi.org/10.3390/cancers15051436

Van den Bosch, T., van Beek, J. G. M., Vaarwater, J., Verdijk, R. M., Naus, N. C., Paridaens, D., … , &Kiliç, E. (2012) 'Higher Percentage of FISH-Determined Monosomy 3 and 8q Amplification in Uveal Melanoma Cells relate to Poor Patient Prognosis.' *Investigative Opthalmology & Visual Science, 53(6), 2668.* doi:10.1167/iovs.11-8697

Van de Nes, J. A. P., Nelles, J., Kreis, S., Metz, C. H. D., Hager, T., Lohmann, D. R., & Zeschnigk, M. (2016) 'Comparing the Prognostic Value of BAP1 Mutation Pattern, Chromosome 3 Status, and BAP1 Immunohistochemistry in Uveal Melanoma.' *The American Journal of Surgical Pathology, 40(6), 796–805.* doi:10.1097/pas.0000000000000645

Van Raamsdonk, C., Bezrookove, V., Green, G., Bauer, J., Gaugler, L., O'Brien, J. M., …, & Bastian B. C. (2009) 'Frequent somatic mutations of *GNAQ* in uveal melanoma and blue naevi.' *Nature,* 457, 599–602. https://doi.org/10.1038/nature07586

Van Raamsdonk, C. D., Griewank, K. G., Crosby, M. B., Garrido, M. C., Vemula, S., Wiesner, T., …, & Bastian, B. C. (2010). Mutations in GNA11 in uveal melanoma. *The New England journal of medicine*, *363*(23), 2191–2199. https://doi.org/10.1056/NEJMoa1000584

Virgili, G., Gatta, G., Ciccolallo, L., Capocaccia, R., Biggeri, A., Crocetti, E., (…), Paci, E. (2007) ´Incidence of uveal melanoma in Europe´. *Ophthalmology*, 114(12), 2309–2315. https://doi.org/10.1016/j.ophtha.2007.01.032

Weis, E., Shah, C. P., Lajous, M., Shields, J. A., & Shields, C. L. (2006) 'The Association Between Host Susceptibility Factors and Uveal Melanoma: A Meta-analysis.' *Arch Ophthalmol.*,124(1), 54–60. doi:10.1001/archopht.124.1.54

Weis, E., Shah, C. P., Lajous, M., Shields, J. A., & Shields, C. L. (2009) 'The Association of Cutaneous and Iris Nevi with Uveal Melanoma: A Meta-analysis.' *Ophthalmology, 116(3), 536–543.e2.* doi:10.1016/j.ophtha.2008.10.008

Welsch, U., Kummer, W., Deller, T. (2022) *Histologie - das Lehrbuch: Zytologie, Histologie und mikroskopische Anatomie* (6., umfassend aktualisierte Auflage.). München: Urban & Fischer in Elsevier.

White, J. S., Becker, R. L., McLean, I. W., Director-Myska, A. E., & Nath, J. (2006) ´Molecular cytogenetic evaluation of 10 uveal melanoma cell lines´. *Cancer genetics and cytogenetics*, *168*(1), 11–21. https://doi.org/10.1016/j.cancergencyto.2005.11.016

Yamaguchi, Y., & Hearing, V. J. (2014) 'Melanocytes and their diseases.' *Cold Spring Harbor perspectives in medicine*, *4*(5), a017046. https://doi.org/10.1101/cshperspect.a017046

Yavuzyigitoglu, S., Koopmans, A. E., Verdijk, R. M., Vaarwater, J., Eussen, B., van Bodegom, A., …, &de Klein, A. (2016) 'Uveal Melanomas with SF3B1 Mutations.' *Ophthalmology, 123(5), 1118–1128.* doi:10.1016/j.ophtha.2016.01.023

Zhao, Z., Bauer, N., Aleksandrowicz, E., Yin, L., Gladkich, J., Gross, W., …, & Herr, I. (2018) 'Intraductal papillary mucinous neoplasm of the pancreas rapidly xenografts in chicken eggs and predicts aggressiveness.' *International journal of cancer*, *142*(7), 1440–1452. https://doi.org/10.1002/ijc.31160